Proposal of Novel Spindle Speed Variation Profile with Constant Acceleration Rate for Improvement of Chatter Stability

Soohyun Nam[a,*], Takehiro Hayasaka[a], Hongjin Jung[a], and Eiji Shamoto[a]

[a] Department of Aerospace Engineering, Graduate School of Engineering, Nagoya University, Furo-cho, Chikusa-ku, Nagoya, 464-8603, Japan.

Abstract

Spindle speed variation (SSV) is one of the effective methods which suppresses regenerative chatter. However, regenerative chatter can grow even if SSV is applied. In the previous work, the chatter growth characteristics in SSV were clarified. The chatter frequency changes proportionally to the varying spindle speed, and it causes the change of the magnitude of the dynamic compliance. Hence, chatter can be suppressed through SSV since the dynamic compliance usually reduces as the chatter frequency changes. A greater compliance reduction can be obtained by a higher rate of spindle speeds in two consecutive revolutions at the same angular position, i.e., acceleration rate. From the investigations in the previous work, limitation of the conventionally utilized SSV profiles is found as follows: the acceleration rate always fluctuates with speed variation and the chatter vibration grows where the acceleration rate is insufficient for suppression, and hence suppressing chatter in all sections of SSV is difficult. In this paper, a new SSV profile with a constant acceleration rate, namely CAR-SSV, is proposed to overcome the limitation of chatter stability improvement by utilizing conventional SSV profiles. The magnitude of the acceleration rate is kept constant to realize the chatter suppression effect throughout the cutting process. Through time-domain simulation and cutting experiments, the chatter stability of CAR-SSV is investigated based on the previously introduced chatter stability evaluation indices. Influence of the parameters of CAR-SSV on the stability is investigated, and an appropriate strategy for setting SSV parameters to achieve higher stability is discussed. In addition, in order to verify the effectiveness of the proposed profile, the stabilities of conventional SSV profiles and CAR-SSV are compared through time-domain simulations and cutting experiments.

Keywords: Regenerative chatter; Spindle speed variation; Acceleration rate; Cutting; Stability.

1 Introduction

Regenerative chatter [1] is one of the most common obstacles in the cutting process which causes poor surface finish and damage of cutting tools. Therefore, the cutting width is limited, which leads to smaller productivity. Regenerative chatter is caused by the regeneration of the previous vibration which is left on the workpiece as a wavy surface. When vibration occurs during cutting, the phase shift between the present and previous vibrations causes dynamic chip load. This dynamic load then excites the vibratory structure, and hence chatter grows up. Extensive studies have been conducted to realize chatter suppression [2-3]. Improving the design of the machine tool or cutting tool can expand the chatter-free zones [2]. For example, a specially designed cutting tool system to improve the damping capacity [4] and a special milling tool which can disrupt the regenerative effect with irregular pitch angle [5] or helix angle [6] were studied. Chatter can also be suppressed by adopting appropriate spindle speed [7] and rake/clearance angles [8] or utilizing actuators [9, 10].

SSV is one of the effective and practical techniques for regenerative chatter suppression [11]. However, regenerative chatter can grow even if SSV is applied [12-15] when the SSV parameters, i.e., nominal spindle speed, variation amplitude, and variation period, are set inappropriately. In the previous work [15], the chatter growth characteristics in the conventional SSV profiles, e.g., sinusoidal spindle speed variation (SSSV) and triangular spindle speed variation (TSSV), were clarified. When chatter occurs during cutting with SSV, it is found that the time chatter frequency changes at the same ratio as the spindle speed, meaning that the spatial frequency is kept constant (the first chatter growth characteristic) [15]. Here, the spatial chatter frequency denotes the number of waves which is left on the cut surface per radian due to the

regenerative chatter. The change of the time chatter frequency causes the change of the magnitude of the dynamic compliance, and hence the chatter can be suppressed since the dynamic compliance usually reduces as the chatter frequency changes. Note that a greater compliance reduction can be obtained by a higher rate of spindle speeds in two consecutive revolutions at the same angular position [15], i.e., acceleration rate, and thus the chatter grows where the acceleration rate is insufficient for suppressing the chatter (the second chatter growth characteristic).

Based on the magnitude of the compliance reduction, two novel indices to evaluate the chatter stability of SSV were proposed [15]. The first one is the average of the absolute acceleration rate in one period of SSV, and the second one is the number of revolutions in a unidirectional acceleration section. Their validity was verified through time-domain simulations and cutting experiments. On the other hand, it has been found that conventional SSV profiles has a limitation as follows: the acceleration rate always fluctuates in conventional SSV profiles, and hence suppressing chatter in all sections of SSV is difficult since the magnitude of chatter suppression effect changes during the speed variation. Especially, the acceleration rate decreases in a high-speed region, and thus remarkable improvement of machining efficiency cannot be realized.

In this paper, a novel SSV which maintains a constant absolute acceleration rate, namely CAR-SSV, is proposed to overcome the limitation of the conventional SSV. Specifically, it is expected that the chatter stability can be improved in all speed regions by maintaining the absolute acceleration rate a constant which is higher than the critical value for suppressing chatter.

The concept of CAR-SSV and its formulation are described in Chapter 2. The time-domain simulation model is described in Section 3.1. A comparison of the stability of CAR-SSV and conventional SSV is carried out based on the stability indices, and the effects of the CAR-SSV parameters on the stability are investigated to propose the strategies for setting appropriate parameters to improve the stability. They are described in Section 3.2. In Section 3.3, a comparison of TSSV, SSSV, and CAR-SSV focusing on its applicability is carried out to verify the effectiveness of the proposed profile. Experimental verifications are described in Chapter 4, and the conclusions of the paper follow in Chapter 5.

2 Proposal of CAR-SSV

2.1 Concept of CAR-SSV

When chatter grows in cutting, it is transferred to the workpiece as a wavy surface. In the next revolution, the difference between the wavy surface and the present vibratory locus of the cutting edge causes the cutting force fluctuation. As discussed in the previous work [15], the spatial chatter frequency f_{sc} [1/rad] can be defined as a number of waves left on the cut surface per unit angle, see Fig. 1, and it is expressed by Eq. (1). Note that the figure is drawn as a plunge-turning process where the vibration waves can be seen easily, but it is the same in other cutting processes.

$$f_{sc} = \frac{60 f_c(t)}{2\pi n(t)} \tag{1}$$

Here, $n(t)$ [min^{-1}] and $f_c(t)$ [Hz] are the spindle speed and the chatter frequency on the time t, respectively. From Eq. (1), the chatter frequency $f_c(t)$ can be described as follows.

$$f_c(t) = \frac{2\pi n(t) f_{sc}}{60} \tag{2}$$

In the case of constant spindle speed (CSS), $f_c(t)$ is constant since $n(t)$ is constant during the cutting. On the other hand, it was clarified that the regenerative chatter generally grows at a constant spatial frequency in SSV, i.e., the time chatter frequency changes at the same rate of spindle speeds in two consecutive revolutions at the same angular position [15]. The varied time chatter frequency can be expressed as follows,

$$f_c(t) = \frac{n(t)}{n\big(t-\tau(t)\big)} f_c(t-\tau(t)) \tag{3}$$

where $\tau(t)$ [s], $n\big(t-\tau(t)\big)$ [min^{-1}], and $f_c(t-\tau(t))$ [Hz] are the spindle rotational period which varies depending on the spindle speed profile, the spindle speed at one revolution before, and the chatter frequency at one revolution before, respectively.

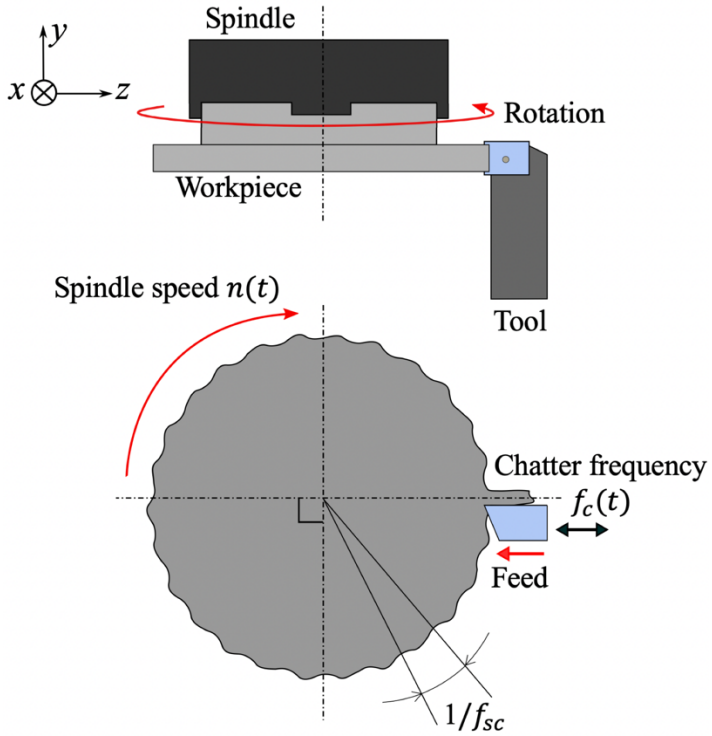

Fig. 1. Schematic illustration of plunge-turning process with regenerative chatter [15].

Since regenerative chatter tends to occur near the resonance, the change of the time chatter frequency causes a reduction of the magnitude of the dynamic compliance of the vibratory structure. A larger compliance reduction can be obtained with a larger change of time chatter frequency. Since the acceleration rate r_a [%] is equivalent to the rate of the change of the time chatter frequency, it was proposed as a key parameter to evaluate the chatter suppression effect by speed variation [14, 15]. For SSV, the average of the absolute acceleration rate in one period of SSV $\overline{|r_a|}$ was proposed as one of the indices to evaluate the chatter stability [15]. In the previous work, r_a [%] and $\overline{|r_a|}$ [%] were defined as follows.

$$r_a(t) = \left(\frac{n(t)}{n\big(t-\tau(t)\big)} - 1\right) \times 100 \tag{4}$$

$$\overline{|r_a|} = \frac{1}{T}\int_0^T |r_a(t)|\, dt \tag{5}$$

In general, the variation amplitude is set high to suppress regenerative chatter when utilizing SSV. This increases the number of revolutions in a unidirectional acceleration section N, which is the second stability index of SSV. However, it has been found that the acceleration rate inevitably fluctuates with this increase, and it becomes small in the high-speed region. Thus, the chatter suppression effect decreases. This is the limitation of the conventional SSV, and a remarkable improvement of the machining efficiency cannot be realized when utilizing them.

To overcome the limitation of the conventional SSV, CAR-SSV, where the absolute acceleration rate is maintained a constant which is higher than the critical value for suppressing chatter, is proposed. It is expected that the chatter stability can be improved in all speed regions.

Examples of the spindle speed and the acceleration rate in CAR-SSV and TSSV are shown in Fig.

2. The red solid and blue dashed lines represent the profiles of CAR-SSV and TSSV, respectively. n_{min}, n_{max}, $n_{0,T}$, and $n_{0,C}$ in the spindle speed profile are the minimum spindle speed, the maximum spindle speed, nominal spindle speed in TSSV, and reference spindle speed in CAR-SSV, respectively. Note that $n_{0,C}$ is defined as the spindle speed at half the time period of a unidirectional acceleration, e.g., spindle speed at $T/4$. To maintain $|r_a|$ constant in the acceleration section in CAR-SSV, the speed change in each revolution becomes larger according to the increase of the spindle speed. In other words, a larger acceleration is necessary for higher spindle speeds, and thus the time period for changing a certain amount of spindle speed will be smaller in the higher spindle speeds compared to the lower spindle speeds. From this reason, the average spindle speeds in TSSV and CAR-SSV denote different values.

In order to make the spindle speed profiles in the acceleration and deceleration sections symmetrical against the spindle speed axis, $|r_a|$ in those sections are maintained unequal as $r_{s,acc}$ and $r_{s,dec}$ shown in the acceleration rate profile of CAR-SSV in Fig. 2. Specifically, assuming that n_h is a high spindle speed and n_l is a low spindle speed, $r_{s,acc}$ and $r_{s,dec}$ can be expressed as $r_{s,acc} = (n_h/n_l - 1) \times 100$ and $r_{s,dec} = (n_l/n_h - 1) \times 100$, respectively. The absolute values of those are unequal. However, the discrepancy between $r_{s,acc}$ and $r_{s,dec}$ is not large since they are usually small values. For instance, when $r_{s,acc}$ is set to 5%, $r_{s,dec}$ is about 4.8%. For the generation of the spindle speed profile, $r_{s,acc}$ is defined first, and then $r_{s,dec}$ is determined subordinately. Therefore, $r_{s,acc}$ will be utilized as set (aimed) acceleration rate r_s [%] in this paper. Note that $r_{s,dec}$ can be set equal to $r_{s,acc}$, but the time period for the acceleration and deceleration sections will differ in that case. In the sections where the acceleration direction switches, i.e., switching from acceleration to deceleration ($= t_{1,C}$) or from deceleration to acceleration ($= t_{2,C}$), $|r_a|$ is close to zero.

As for TSSV, it can be confirmed that r_a in TSSV fluctuates largely throughout the speed variation region. $\pm r_{max,T}$ and $\pm r_{min,T}$ represent the maximum and minimum acceleration rates of TSSV in all sections, respectively, except for the sections where the acceleration direction switches. t_h represents the time length where $|r_a|$ in CAR-SSV is greater than that in TSSV, and t_l represents the time length where $|r_a|$ in CAR-SSV is less than that in TSSV.

Chatter suppression effect throughout the cutting is expected in CAR-SSV since $|r_a|$ is maintained constant regardless of the speed variation except for the sections where the acceleration direction switches. Furthermore, when the critical $|r_a|$ necessary for suppressing the chatter is larger than $|r_{min,T}|$ but smaller than $|r_s|$, chatter can be effectively suppressed throughout the cutting when CAR-SSV is utilized. On the other hand, chatter grows during t_h when TSSV is utilized.

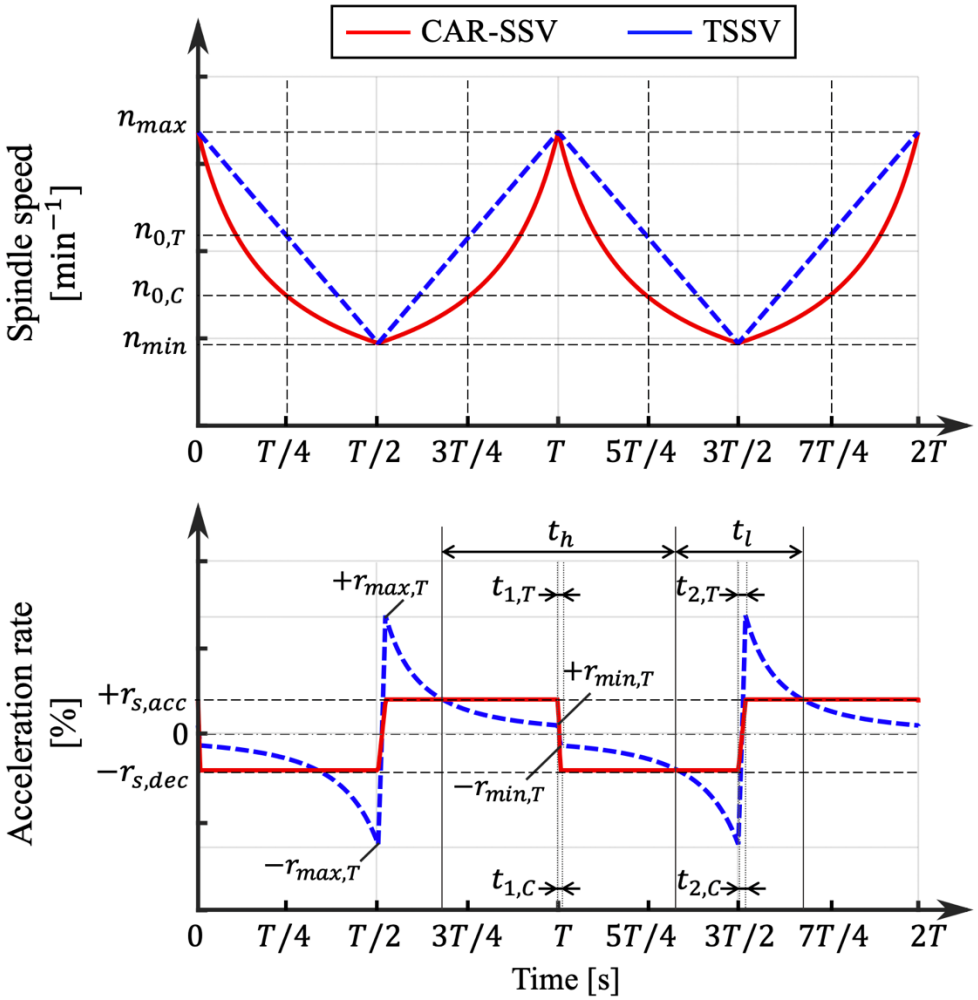

Fig. 2. Profiles of spindle speed and acceleration rate in CAR-SSV and TSSV.

2.2 Formulation of CAR-SSV profile

This section introduces the formulation of the CAR-SSV profile in order to utilize it in the time-domain simulation. The formulations of TSSV and SSSV have been introduced in the previous works [12, 15]. The spindle speed of CAR-SSV in the acceleration section $n_{acc,C}$ [min^{-1}] and the deceleration section $n_{dec,C}$ [min^{-1}] can be formulated as a function of θ as follows:

$$\begin{cases} n_{acc,C}(\theta) = n_{ini}\left(1+\dfrac{r_{s,acc}}{100}\right)^{\frac{\theta}{2\pi}} \\ n_{dec,C}(\theta) = n_{ini}\left(1+\dfrac{r_{s,dec}}{100}\right)^{\frac{\theta}{2\pi}} \end{cases} \tag{6}$$

where n_{ini} [min^{-1}] is the initial spindle speed in that section. The following differential equation in the acceleration section can be obtained:

$$\frac{d\theta}{dt} = \frac{2\pi n_{acc,C}(\theta)}{60} = \frac{2\pi n_{ini}\left(1+\dfrac{r_{s,acc}}{100}\right)^{\frac{\theta}{2\pi}}}{60} \tag{7}$$

This equation can be transformed as follows:

$$\frac{dt}{d\theta} = \frac{60}{2\pi n_{ini}}\left(1+\frac{r_{s,acc}}{100}\right)^{-\frac{\theta}{2\pi}} = \frac{60}{2\pi n_{ini}} e^{-\frac{\theta}{2\pi}\ln\left(1+\frac{r_{s,acc}}{100}\right)} \tag{8}$$

Next, Eq. (9) can be obtained from the integration of Eq. (8):

$$t = \int \frac{dt}{d\theta} d\theta = \frac{60}{2\pi n_{ini}} \int e^{-\frac{\theta}{2\pi}\ln\left(1+\frac{r_{s,acc}}{100}\right)} d\theta = -\frac{60}{n_{ini}\ln\left(1+\frac{r_{s,acc}}{100}\right)} e^{-\frac{\theta}{2\pi}\ln\left(1+\frac{r_{s,acc}}{100}\right)} + C \tag{9}$$

where C is an integral constant, and C can be determined by utilizing the initial condition ($t(0) = 0$) as follows:

$$C = \frac{60}{n_{ini}\ln\left(1+\frac{r_{s,acc}}{100}\right)} \tag{10}$$

From Eqs. (9) and (10), $\theta(t)$ can be calculated as:

$$\theta(t) = -\frac{2\pi}{\ln\left(1+\frac{r_{s,acc}}{100}\right)} \ln\left\{1-\left(\frac{n_{ini}}{60}\ln\left(1+\frac{r_{s,acc}}{100}\right)\right)t\right\} \tag{11}$$

The following differential equation is obtained:

$$\frac{d\theta(t)}{dt} = \frac{2\pi n_{ini}}{60 - \left\{n_{ini}\ln\left(1+\frac{r_{s,acc}}{100}\right)\right\}t} \tag{12}$$

By using Eqs. (7) and (12), $n_{acc,C}(t)$ can be derived as follows:

$$n_{acc,C}(t) = \frac{n_{ini}}{1-\left\{\frac{n_{ini}}{60}\ln\left(1+\frac{r_{s,acc}}{100}\right)\right\}t} \tag{13}$$

In the same manner with Eqs. (7)-(12), the formulation of $n_{dec,C}(t)$ can be derived as:

$$n_{dec,C}(t) = \frac{n_{ini}}{1-\left\{\frac{n_{ini}}{60}\ln\left(1+\frac{r_{s,dec}}{100}\right)\right\}t} \tag{14}$$

In this paper, $r_{s,acc}$ is defined as the set acceleration rate r_s [%].

$|r_a|$ is close to zero at the sections where the acceleration direction switches. Since the angle of these sections is one revolution, i.e., 2π rad, the time lengths t_1 and t_2 satisfy the following equations.

$$\int_{\frac{kT}{2}}^{\frac{kT}{2}+t_1} \frac{n(t)}{60} dt = 1 \qquad (k = 2, 4, 6, 8 \dots) \tag{15}$$

$$\int_{\frac{k'T}{2}}^{\frac{k'T}{2}+t_2} \frac{n(t)}{60} dt = 1 \qquad (k' = 1, 3, 5, 7 \dots) \tag{16}$$

3 Analytical investigations of CAR-SSV

3.1 Time-domain simulation model

Time-domain simulations are carried out to investigate the influence of the parameters of CAR-SSV on the chatter stability and to verify the validity of CAR-SSV through comparison with SSSV and TSSV. Fig. 3 shows a schematic illustration of the dynamic model in a SDOF vibratory system. It is assumed that the cutting tool is flexible in the thrust (z) direction, and the regeneration occurs only in the z direction. The dynamic uncut chip thickness $h(t)$ [m] and dynamic cutting force in the thrust direction $F_z(t)$ [N] can be expressed as follows:

$$h(t) = h_0 + \mu z\big(t-\tau(t)\big) - z(t) = h_0 + \mu z(\theta(t)-2\pi) - z(t) \tag{17}$$

$$F_z(t) = K_z a h(t) \tag{18}$$

where h_0 [m] is the static depth of cut, μ is the overlapping factor ($\mu = 1$ in orthogonal cutting process such as pipe-plunging), $\tau(t)$ [s] is the time-varying spindle rotational period, $z(t)$ [m] is the dynamic

displacement, $\theta(t)$ [rad] is the spindle rotational angle, $z(\theta(t)-2\pi)$ is the dynamic displacement of one revolution before at the spindle rotational angle $\theta(t)$, K_z [Pa] is the specific cutting force in the thrust direction, and a [m] is the cutting width.

The equation of motion of the tool can be expressed as follows:

$$m\ddot{z}(t)+c\dot{z}(t)+kz(t)=K_z a(h_0+\mu z(\theta(t)-2\pi)-z(t)) \tag{19}$$

where m [kg], c [N/(m·s)], and k [N/m] are the modal mass, damping coefficient, and stiffness of the tool, respectively. The time-varying spindle rotational period $\tau(t)$ can be calculated by the following equation.

$$\int_{t-\tau(t)}^{t}\frac{n(t)}{60}dt=1 \tag{20}$$

In the time-domain simulation, $z(t)$ is calculated by solving Eq. (19) directly, and the solution is approximated by the 4th order Runge-Kutta method. In order to calculate $\theta(t)$, $z(\theta(t)-2\pi)$, and $r_a(t)$, the values of $z(t)$ and $n(t)$ at each calculation step of the time-domain simulation are memorized. For instance, $\theta(t)$ can be calculated by integrating the spindle speed by Eq. (21), and the time difference between the present and previous revolutions at the same angular position $\tau(t)$ is determined by finding the minimum value of K satisfying the following modulo function: $\mathrm{mod}(\theta(t)-\theta(t-K\times t_{res}),2\pi)\fallingdotseq 0$, i.e., $\tau(t)=\min(K)\times t_{res}$, where t_{res} is the time resolution of the simulation.

$$\theta(t)=2\pi\int_0^t\frac{n(t)}{60}dt \tag{21}$$

The static depth of cut gradually increases at the beginning of the simulation, and this is the only source of chatter applied in it. Note that the tool disengagement from the workpiece due to the chatter growth, i.e., $h(t)=0$, and the multiple regenerative effect [16] from this phenomenon are considered in the simulation.

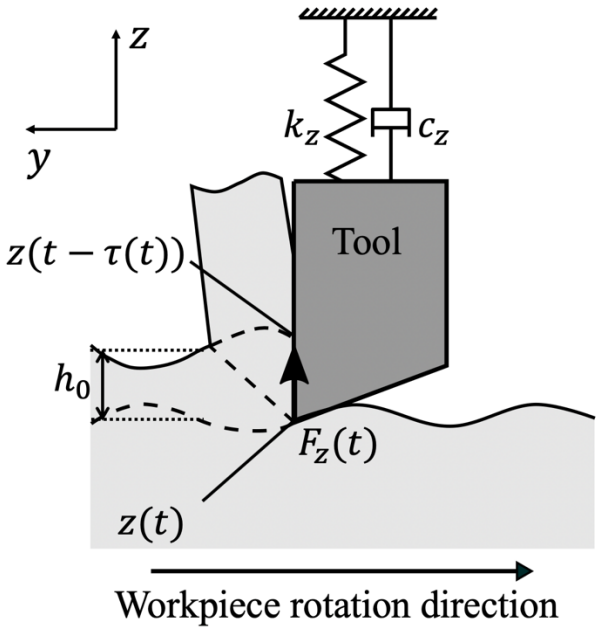

Fig. 3. Schematic illustration of dynamic cutting model with SDOF vibratory system.

3.2 Comparison with conventional SSV based on stability indices and clarification of effects of CAR-SSV parameters on stability

In order to verify the effectiveness of CAR-SSV, a comparison of the stability of CAR-SSV and conventional SSV is carried out based on the stability indices [15], i.e., $\overline{|r_a|}$ and N. The parameters utilized

in the time-domain simulation are shown in Table 1. The cutting width is increased by 0.1 mm increment, and the cutting width where chatter occurs is searched. Note that the growing vibration in each period of SSV is considered as chatter. By subtracting one increment from that width, the stability limit a_{lim} [mm] is determined.

Table 1. Parameters used in time-domain simulation.

Workpiece properties		
Diameter D	[mm]	70
Specific cutting force in thrust direction K_z	[MPa]	711
Modal parameters		
Mass m	[kg]	0.2266
Damping coefficient c	[N/(m·s)]	44.19
Stiffness k	[N/m]	1.118×10^7
Parameters of CAR-SSV		
Reference spindle speed $n_{0,C}$	$[\mathrm{min}^{-1}]$	600-3500
Variation period T	[s]	1.0
Set acceleration rate r_s	[%]	2.5-10.2
Cutting conditions		
Feed rate (static depth of cut) h_0	[mm/rev]	0.05
Cutting width a	[mm]	0.1 – 12.0

Fig. 4 shows the stability limits against the stability indices $\overline{|r_a|}$ and N in (a) SSSV [15], (b) TSSV [15], and (c) CAR-SSV at $T = 1.0$ s. In the case of SSSV and TSSV, $n_{0,S}$ and $n_{0,T}$ is proportional to N at a constant T [15]. Meanwhile, since the average spindle speed in CAR-SSV is different from $n_{0,C}$, the values of $n_{0,C}$ and r_s in CAR-SSV at each condition in Fig. 4(c) that satisfy the defined values of $\overline{|r_a|}$ and N are searched. The magnitude of the stability limit (critical cutting width) is represented by utilizing a color map. From Fig. 4, the following remarks are found.

1) When $\overline{|r_a|}$ and N are the same, the stability limit of CAR-SSV is always equal to or higher than those of SSSV and TSSV. The increase of the stability limit of CAR-SSV to those of SSSV and TSSV at each condition is calculated. From the result, it is confirmed that the larger the $\overline{|r_a|}$ and N, the larger the increase. Especially, the stability limit at $\overline{|r_a|} = 10$ % and $N = 30$ in CAR-SSV (a_C in Fig. 4(c)) is about 2.70 times those of SSSV (a_S in Fig. 4(a)) and TSSV (a_T in Fig. 4(b)).
2) When N is the same, the stability limit increases with an increase of $\overline{|r_a|}$ regardless of the type of SSV.
3) When $\overline{|r_a|}$ is the same, the stability limits of SSSV and TSSV are the largest at a certain N, e.g., 20 in the case of $\overline{|r_a|} = 10$, but the stability limit of CAR-SSV increases with an increase of N under all $\overline{|r_a|}$. The reason for this can be considered as follows. In the cases of SSSV and TSSV, the fluctuation amplitude of $|r_a|$ becomes large with an increase of N [15], and hence the chatter can grow when $|r_a|$ is insufficient to suppress the chatter. In contrast, when utilizing CAR-SSV, $|r_a|$ is sufficient in almost all sections since $|r_a|$ is kept constant except for the sections where the acceleration direction switches. Therefore, a larger change of chatter frequency can be obtained with a larger N, and it increases the stability limit.

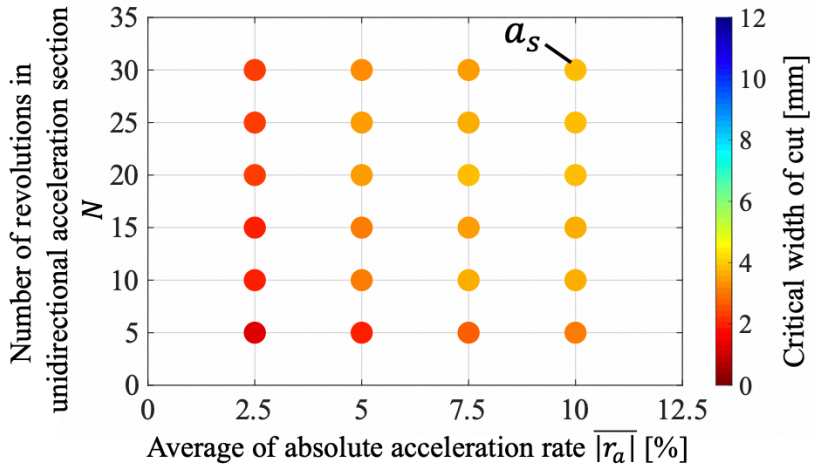

(a) SSSV, $T = 1.0$ s

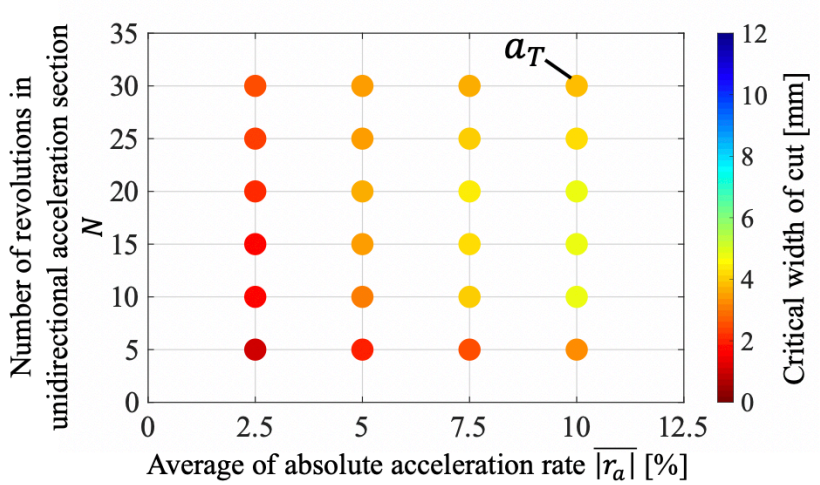

(b) TSSV, $T = 1.0$ s

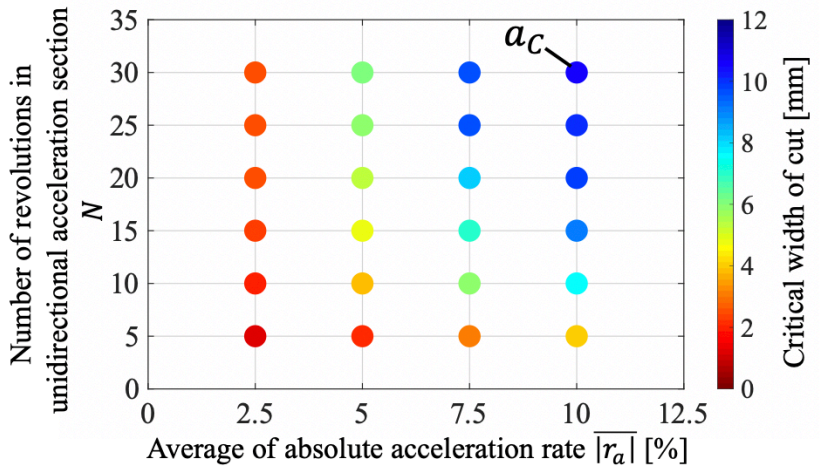

(c) CAR-SSV, $T = 1.0$ s

Fig. 4. Stability limits against stability indices $\overline{|r_a|}$ and N in (a) SSSV, (b) TSSV, and (c) CAR-SSV at $T = 1.0$ s.

Next, the relations between the CAR-SSV parameters and the stability are investigated to propose

the strategies for setting appropriate parameters. The parameters of CAR-SSV utilized in investigation are shown in Table 2. Fig. 5 shows the simulation results at multiple variation periods: (a) $T = 0.5$ s, (b) $T = 1.0$ s, (c) $T = 2.0$ s, and (d) $T = 4.0$ s. Each graph represents the stability limit against the acceleration rate. The black dotted line with crosses represents the results at $n_{0,C} = 1000$ min^{-1}, the blue dashed line with triangles represents the results at $n_{0,C} = 1500$ min^{-1}, and the red solid line with circles represents the results at $n_{0,C} = 2000$ min^{-1}. Figs. 6 (a), (b), and (c) show the profiles of the spindle speed $n(t)$, the acceleration rate $r_a(t)$, and the spindle rotational angle $\theta(t)$ which correspond to A, B, and C marked on Fig. 5, respectively. Here, the set acceleration rate r_s in the three profiles are the same, i.e., 3 %, but $n_{0,C}$ and T are different: (a) $n_{0,C} = 1000$ min^{-1}, $T = 0.5$ s, (b) $n_{0,C} = 2000$ min^{-1}, $T = 0.5$ s, and (c) $n_{0,C} = 1000$ min^{-1}, $T = 4.0$ s. Note that even if $n_{0,C}$ and r_s are the same, the larger the T, the higher the maximum spindle speed and the lower the minimum spindle speed as shown in Figs. 6 (a) and 6 (c). From the results, the following remarks are found.

Table 2. Parameters of CAR-SSV used in time-domain simulation.

Parameters of CAR-SSV		
Reference spindle speed $n_{0,C}$	[min^{-1}]	1000, 1500, 2000
Variation period T	[s]	0.5, 1.0, 2,0, 4.0
Set acceleration rate r_s	[%]	1, 2, 3, 4, 5, 6

1) The stability limit increases with a higher r_s under most $n_{0,C}$ and T, except for when r_s increases from 5 % to 6 % at $T = 4.0$ s shown in Fig. 5(d). Hence, in order to increase the chatter stability, it is desirable to set a larger r_s as long as the limit of the spindle motor load is not exceeded.
2) When r_s is the same, the stability limit mostly increases with an increase of $n_{0,C}$ and T. To investigate this reason, $\overline{|r_a|}$ [%] and N of the profiles shown in Fig. 6 are evaluated. Note that N is calculated as follows:
$$N = \frac{\int_{T/2}^{T} \theta(t)\, dt}{2\pi} = \frac{\int_{T}^{3T/2} \theta(t)\, dt}{2\pi} \tag{22}$$
t_1 is the time period of the section where the acceleration directions switches from deceleration to acceleration, t_2 is the time period of the section where the acceleration direction switches from acceleration to deceleration, t_3 is the time period of the acceleration section, and t_4 is the time period of the deceleration section. The calculated values of ($\overline{|r_a|}$, N) at the conditions of A, B, and C are (2.68 %, 4.18), (2.86 %, 8.35), and (2.99 %, 36.1), respectively. From these, it is confirmed that the larger the $n_{0,C}$ and T, the larger the $\overline{|r_a|}$ and N even though the set value r_s is the same. Thus, the stability increases because the chatter frequency can be greatly changed, and the dynamic compliance can be greatly reduced. Assuming the initial chatter frequency f_0, the change of chatter frequency can be expressed as $f_0 \times (1 + r_s/100)^N$. The value of $(1 + r_s/100)^N$ at A, B, and C are 1.12, 1.27, and 2.90, respectively. The dominant reason for the reduction of the compliance is the increase of N because $\overline{|r_a|}$ in all conditions show a similar value. One more reason can be the increase of $\overline{|r_a|}$ from the decrease of t_1 and t_2, which means that the length of the section where $|r_a|$ is insufficient decreases as shown in Fig. 6. For reference, the ratio of the sum of the time periods where the acceleration direction changes $(t_1 + t_2)$ to the sum of the time periods where r_a is maintained a constant $(t_3 + t_4)$ is calculated. The calculated $(t_1 + t_2)/(t_3 + t_4)$ at the conditions of A, B, and C are 0.3256, 0.1358, and 0.0312, respectively. From these two reasons, by setting a large $n_{0,C}$ and T, a remarkable improvement of the machining efficiency can be realized by utilizing CAR-SSV since a large cutting width, i.e., large stability limit, can be adopted. Hence, CAR-SSV can be an effective solution to overcome the limitation of conventional SSV.
3) The tendency of the increase of the stability with a higher $n_{0,C}$ is not confirmed at $T = 4.0$ s. This is thought to happen because the chatter frequency changes excessively due to an extremely large

N at a large T. More specifically, when the chatter frequency excessively changes from the resonance, the reduction effect of the dynamic compliance reaches a certain asymptotic value since the compliance is nearly constant far away from the resonance. Therefore, the increase of the stability against the increase of N becomes smaller.

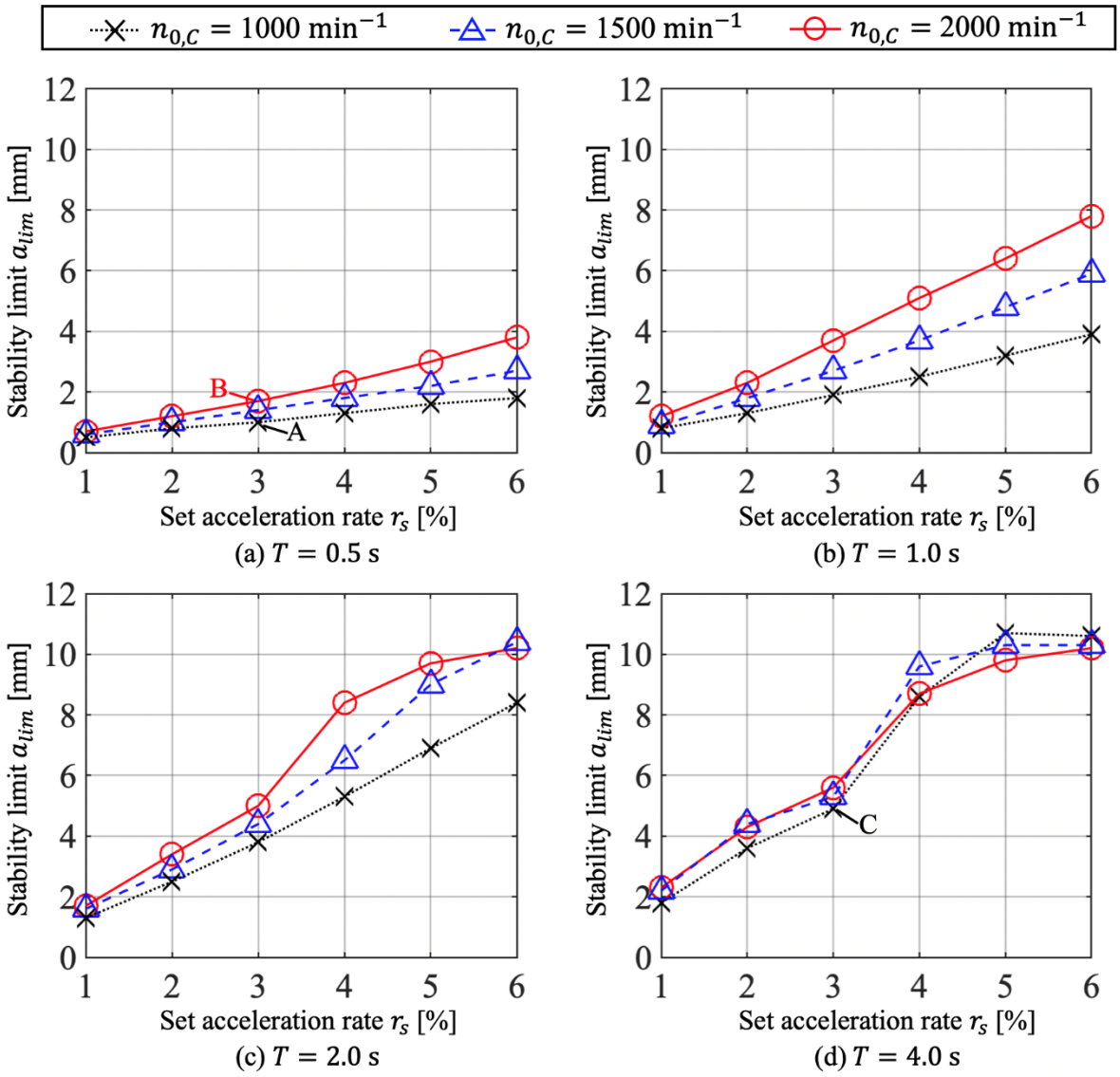

Fig. 5. Stability limits against acceleration rate under varied $n_{0,C}$ and T.

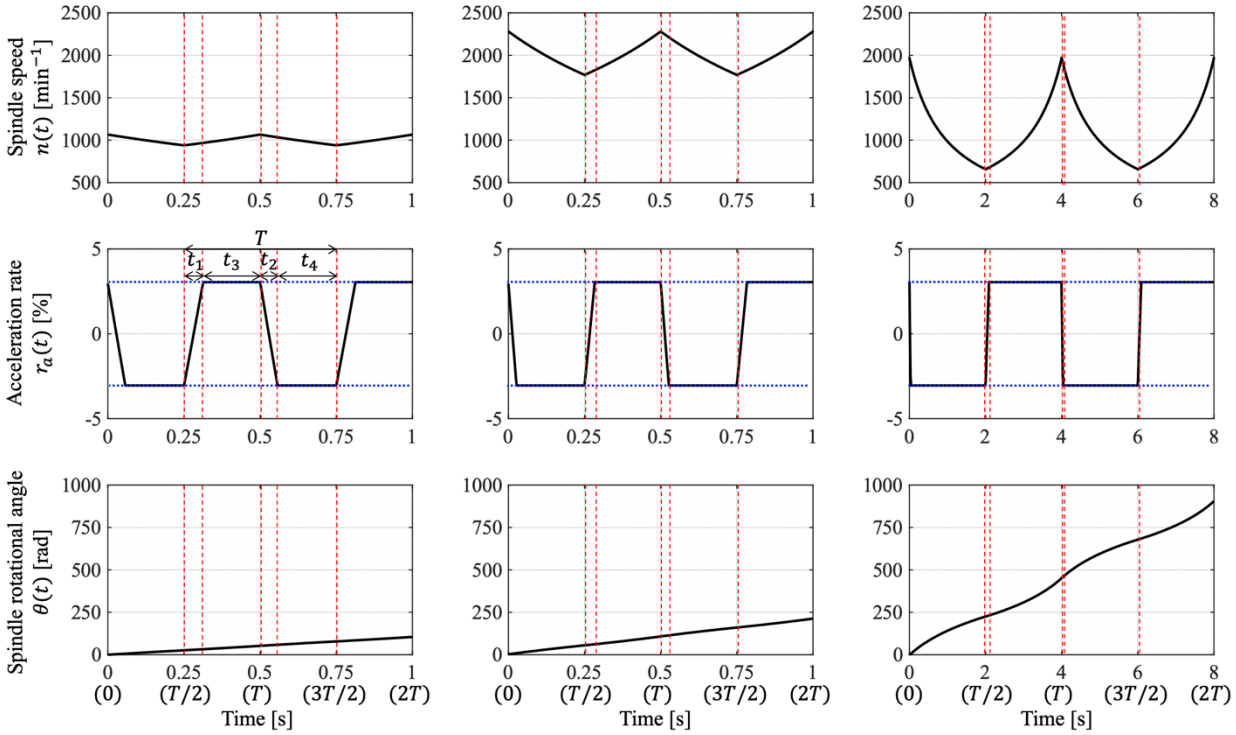

(a) A in Fig. 4 : a_{lim} = 1.0 mm, $n_{0,C}$ = 1000 min^{-1}, T = 0.5 s, $\overline{|r_a|}$ = 2.68 %, N = 4.18

(b) B in Fig. 4 : a_{lim} = 1.7 mm, $n_{0,C}$ = 2000 min^{-1}, T = 0.5 s, $\overline{|r_a|}$ = 2.86 %, N = 8.35

(c) C in Fig. 4 : a_{lim} = 4.9 mm, $n_{0,C}$ = 1000 min^{-1}, T = 4.0 s, $\overline{|r_a|}$ = 2.99 %, N = 36.1

Fig. 6. Profiles of spindle speed, acceleration rate, and spindle rotational angle.

3.3 Comparison with conventional SSV focusing on its applicability

To verify the effectiveness of CAR-SSV focusing on its applicability to the actual industry, the machining efficiency against the thermal load of the spindle motor in CAR-SSV, TSSV, and SSSV are compared.

The spindle speeds of TSSV $n_T(t)$ [min^{-1}] and SSSV $n_S(t)$ [min^{-1}] can be described as follows.

$$n_T(t) = \begin{cases} n_{0,T} + n_{A,T} - \dfrac{4n_{A,T}}{T}\bmod(t,T) & if \quad 0 \le \bmod(t,T) < T/2 \\ n_{0,T} - 3n_{A,T} + \dfrac{4n_{A,T}}{T}\bmod(t,T) & if \quad T/2 \le \bmod(t,T) < T \end{cases} \tag{23}$$

$$n_S(t) = n_{0,S} + n_{A,S}\sin\left(\frac{2\pi}{T}t + \frac{\pi}{2}\right) \tag{24}$$

Here, $n_{0,T}$ [min^{-1}] and $n_{0,S}$ [min^{-1}] are the nominal spindle speeds in TSSV and SSSV, respectively, and $n_{A,T}$ [min^{-1}] and $n_{A,S}$ [min^{-1}] are the variation amplitudes in TSSV and SSSV, respectively. The profiles of CAR-SSV are created at first, and then the profiles of TSSV and SSSV are created with identical thermal load and identical average spindle speed as those of CAR-SSV so that the three profiles can be compared from a practical viewpoint. As a first step, the average spindle speed of CAR-SSV n_{ave} [min^{-1}] is calculated by Eq. (25), and $n_{0,T}$ and $n_{0,S}$ are set equal to n_{ave}.

$$n_{ave} = \frac{2}{T}\int_{T/2}^{T} n_{acc,C}(t)\,dt \tag{25}$$

The thermal load of the spindle motor is basically proportional to the square of the current. Since the current increases proportionally to the spindle acceleration, the thermal load of the spindle motor increases proportionally to the square of the acceleration. Hence, the average of the square of the spindle

acceleration $\overline{H}$ [rev^2/s^4] is equivalent to the average thermal load increase of the spindle motor. The average of the square of the spindle acceleration in SSV $\overline{H}$ [rev^2/s^4] can be calculated as follows.

$$\overline{H} = \frac{2}{T}\int_{\frac{T}{2}}^{T}\left(\frac{d}{dt}\frac{n(t)}{60}\right)^2 dt \tag{26}$$

$\overline{H}$ in CAR-SSV is calculated, and then $n_{A,T}$ and $n_{A,S}$ are determined to satisfy the following relations in order to set the same thermal load from Eqs. (23)-(26).

$$n_{A,T} = 15T\sqrt{\overline{H}} \tag{27}$$

$$n_{A,S} = \frac{30T\sqrt{2\overline{H}}}{\pi} \tag{28}$$

The utilized parameters of CAR-SSV are shown in Table 2 and the parameters of TSSV and SSSV are determined by Eqs. (26)-(28). The machining efficiency P [mm^3/min] is defined with material removal rate (MRR) as follows:

$$P = a_{lim}\pi D h_0 n_{ave} \tag{29}$$

As shown in Table 1, D and h_0 are fixed values which are set the same as those in the experimental conditions. Fig. 7 shows the obtained P against $\overline{H}$ in the three types of SSV under varied T: (a) $T = 0.5$ s, (b) $T = 1.0$ s, (c) $T = 2.0$ s, and (d) $T = 4.0$ s. Red circles represent the results of CAR-SSV, blue triangles represent the results of TSSV, and green crosses represent the results of SSSV. Note that the variation amplitudes of TSSV and SSSV should be set smaller than their average spindle speeds because the spindle speed cannot be lower than 0 min^{-1}. Therefore, the conditions which do not satisfy this constraint are neglected, and those are not plotted in Fig. 7.

Fig. 8 shows the profiles of the spindle speed and the acceleration rate in CAR-SSV, TSSV, and SSSV which correspond to A, B, and C marked on Fig. 7: (A) $T = 0.5$ s, $n_{0,C} = 1000$ min^{-1}, and $r_s = 3$ %, (B) $T = 0.5$ s, $n_{0,C} = 2000$ min^{-1}, and $r_s = 6$ %, and (C) $T = 2.0$ s, $n_{0,C} = 1000$ min^{-1}, and $r_s = 3$ %. From Figs. 7 and 8, the following remarks are found.

1) When $\overline{H}$ is the same, P of CAR-SSV is almost equal to or higher than those of TSSV and SSSV. It is verified that CAR-SSV is more effective to suppress chatter, and the applicability to the actual industry is superior to that of the conventional SSV profiles.
2) From Fig. 7, it is confirmed that the increase of the machining efficiency in CAR-SSV compared to those of TSSV and SSSV becomes larger with a larger $\overline{H}$ and T. The reason for this can be explained as follows. As shown in Fig. 8, the larger the $\overline{H}$ and T, the larger the fluctuation amplitude of r_a in TSSV and SSSV. Consequently, the sections where $|r_a|$ in TSSV and SSSV is smaller than $|r_a|$ in CAR-SSV (near the transitions from acceleration to deceleration) becomes longer. Hence, the change of chatter frequency becomes smaller in those sections in TSSV and SSSV, and the stabilization effect decreases since a sufficient compliance reduction cannot be obtained. In contrast, in the case of CAR-SSV, the time periods t_1 and t_2 of the sections where $|r_a|$ decreases, i.e., the transitions of the acceleration direction, become shorter with a larger $\overline{H}$ and T, and thus CAR-SSV can overcome the limitation of TSSV and SSSV.

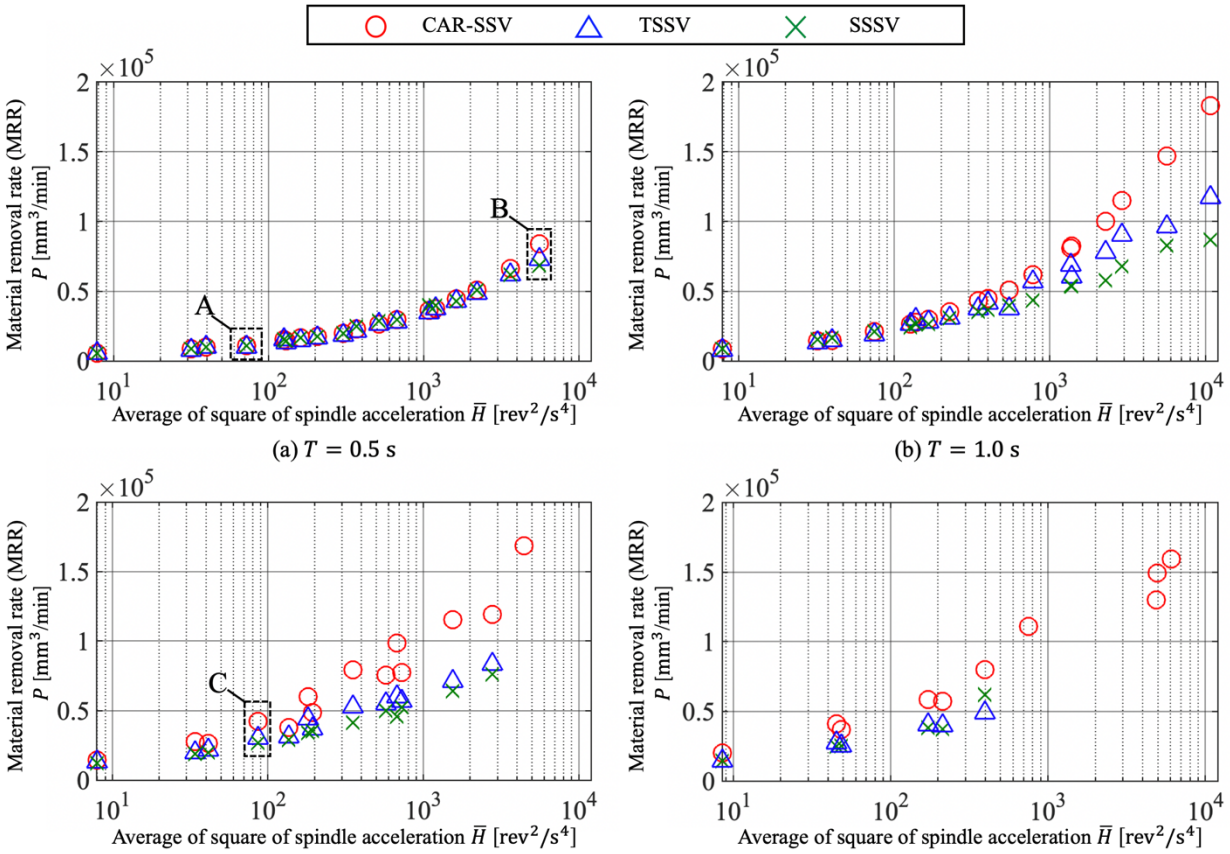

Fig. 7. Simulation results of material removal rate (MRR) P against average of square of spindle acceleration $\bar{H}$ under varied T.

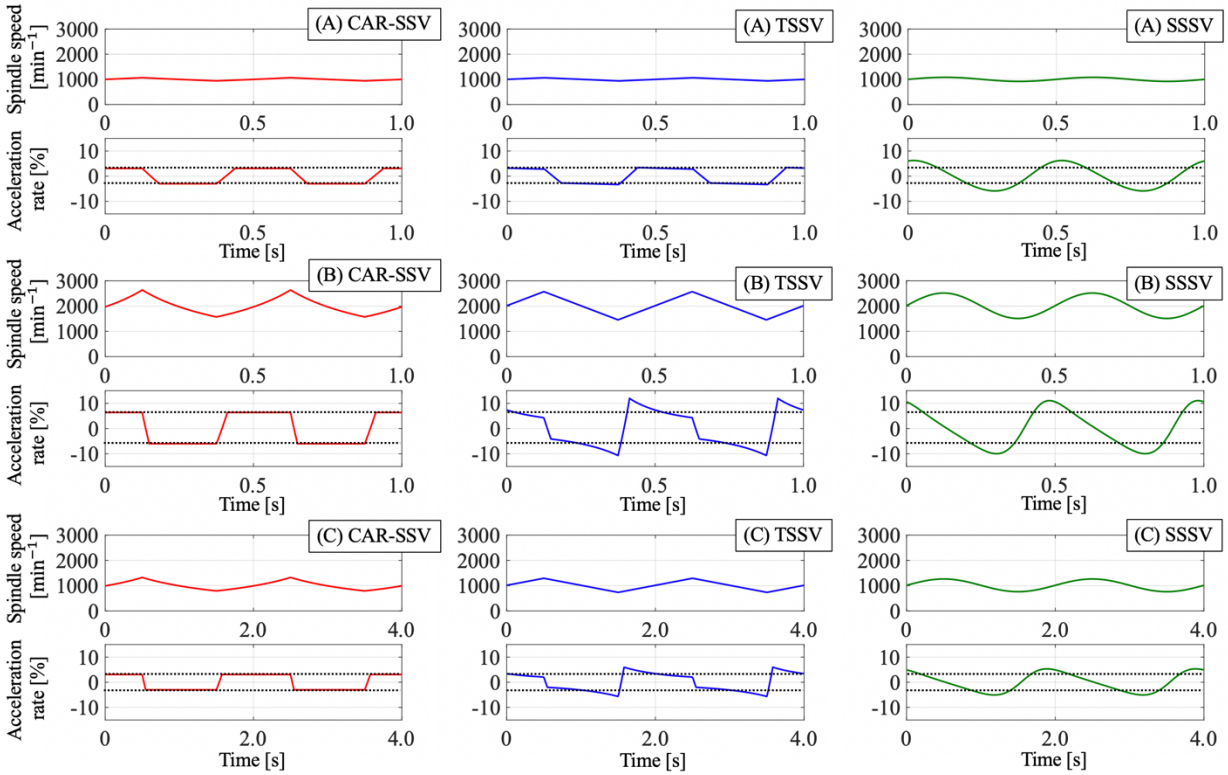

Fig. 8. Profiles of spindle speed and acceleration rate corresponding to A, B, and C marked in Fig. 7.

4 Experimental investigations into CAR-SSV

4.1 Experimental setup

Two series of experiments are carried out to verify the effectiveness of CAR-SSV. Fig. 9 shows a photograph of the experimental setup for the pipe-end plunging and Table 3 shows experimental conditions for two series of experiments. A 2-turret CNC lathe (Okuma Corp., SIMUL TURN LU3000EX) is utilized, and a tool insert (Mitsubishi Material Corp., TCMW16T308 HTi10) mounted on a tool shank (steel, ISO C45) with a rectangular cross-section is used to cut a pipe-shaped workpiece (brass, ISO CuZn35). The rake and clearance angles of the tool are 0 and 7 deg, respectively. The spindle speed and vibration acceleration signals are obtained from the spindle motor encoder and a 3-axis accelerometer mounted on the tool shank, respectively.

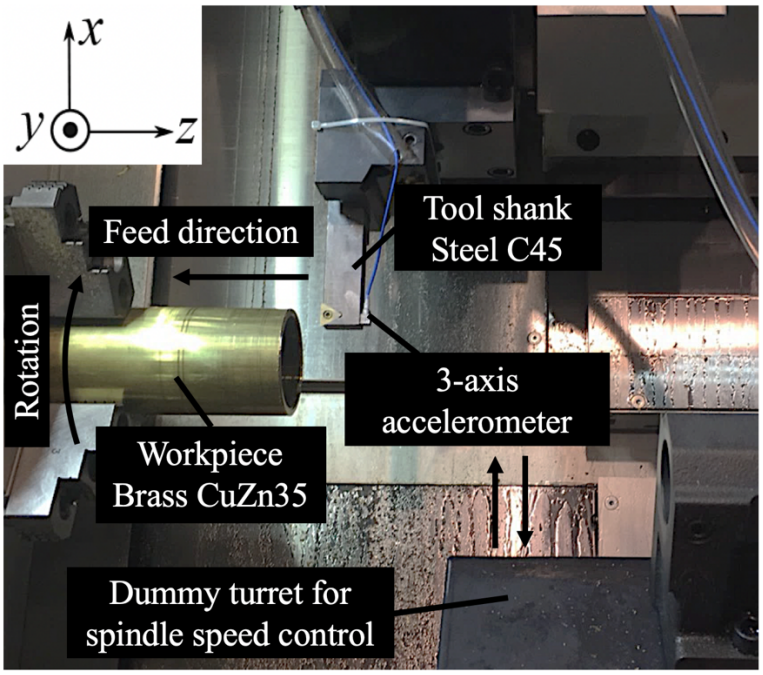

Fig. 9. Experimental setup for pipe-end plunging.

Table 3. Experimental conditions for two series of experiments

Tool		
Tool insert information		Mitsubishi Material Corp. TCMW 16T308 HTi10
Tool shank material		Steel, ISO C45
Rake angle	[deg]	0
Clearance angle	[deg]	7
Workpiece		
Workpiece material		Brass, ISO CuZn35

4.2 Measurement of dynamic compliance of tool shank

The dynamic compliance of the tool shank is measured with an impact hammer (PCB Electronics Inc., 086E80), an accelerometer (PCB Electronics Inc., 356A01), and a dummy tool insert with flat perpendicular faces. These faces are perpendicular to the principal and thrust directions, and they are utilized for accurate force input. The width and the height of the utilized tool is 25 mm and 15 mm, respectively. The projection of the tool shank is set as long as 80 mm, and the workpiece is rigid in the z direction. The impact for each direction is repeated 10 times, and their average is utilized for higher reliability of the measurement. After the measurement of the dynamic compliances, their modal parameters are identified in order to utilize them in the time-domain simulations and compare the results with those of the cutting experiments. The details of the identification of the modal parameters are described in the previous work [15]. The identified modal parameters are shown in Table 4.

The measured and fitted dynamic compliances are shown in Fig. 10, where (a) shows the cross dynamic compliance G_{zy} and (b) shows the direct dynamic compliance G_{zz}. The equivalent dynamic compliance [15, 17] in the thrust direction $G_z(s)$ is calculated by utilizing Eq. (30), and the measured and fitted equivalent dynamic compliances are shown in Fig. 11. Here, K_y and K_z in Eq. (30) are the specific cutting forces in the principal (y) and thrust (z) directions, respectively, and they are measured in advance.

The dashed blue lines and the solid red lines in Figs. 10 and 11 represent the measured and fitted dynamic compliances, respectively.

$$G_z(s) = \{G_{zy}\ G_{zz}\}\begin{Bmatrix} K_y/K_z \\ 1 \end{Bmatrix} = K_y/K_z \times G_{zy} + G_{zz} \tag{30}$$

Table 4. Numerically identified modal parameters.

Modal mass		
m_{yy}	[kg]	0.0658
m_{yz}	[kg]	0.0221
m_{zy}	[kg]	-0.0107
m_{zz}	[kg]	0.1807
Modal damping coefficient		
c_{yy}	[N/(m·s)]	32.73
c_{yz}	[N/(m·s)]	-42.28
c_{zy}	[N/(m·s)]	13.61
c_{zz}	[N/(m·s)]	84.99
Modal stiffness		
k_{yy}	[N/m]	8.203×10^{6}
k_{yz}	[N/m]	2.624×10^{6}
k_{zy}	[N/m]	-5.478×10^{5}
k_{zz}	[N/m]	2.076×10^{7}

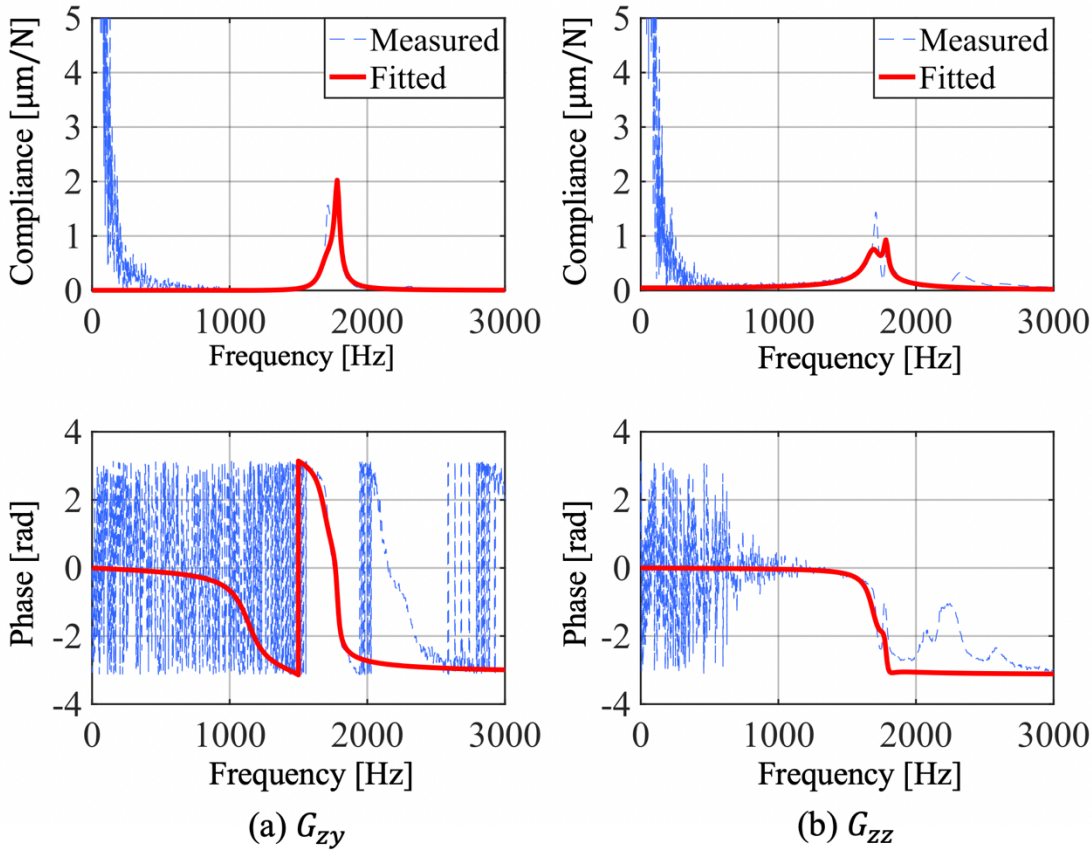

Fig. 10. Measured and fitted dynamic compliances: (a) cross dynamic compliance and (b) direct dynamic compliance.

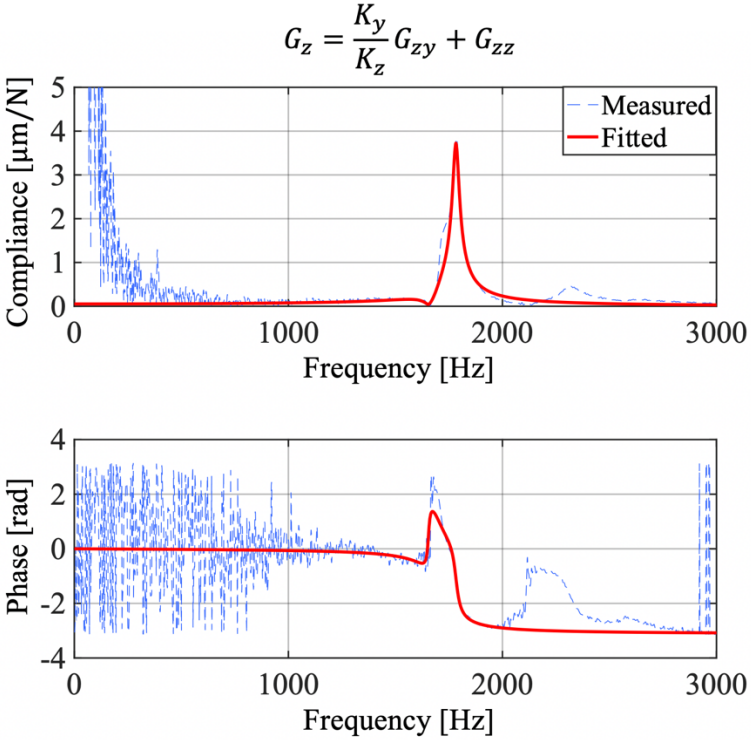

Fig. 11. Measured and fitted equivalent dynamic compliances.

4.3 Cutting experiments with constant spindle speed

Cutting experiments with constant spindle speed (CSS) are conducted to confirm the validity of the dynamic compliance by means of comparing the predicted and experimental stability limits. In addition, the degree of the stability improvement by utilizing CAR-SSV and TSSV compared to CSS can be investigated by comparing the stability limits.

Experimental conditions for cutting with CSS are shown in Table 5. The feed rate, i.e., static depth of cut in pipe-end plunging, is fixed to 0.05 mm, the cutting width, i.e., the thickness of the pipe, is changed by means of pre-cutting, and the spindle speeds are set variable from 1000 to 3000 [min^{-1}]. The stability limits are calculated by utilizing the measured and fitted equivalent dynamic compliances. The predicted stability limits and experimental results are shown in Fig. 12. The blue and red solid lines represent the predicted stability limit with the measured and fitted compliances, respectively. As for the experimental results, the measured vibration acceleration is short-time Fourier transformed to confirm the chatter frequency and the maximum vibration amplitude a_{max}. The circles and the crosses in Fig. 12 represent the cutting results without chatter ($a_{max} < 1.0\ \mu m_{0-p}$) and with chatter ($1.0\ \mu m_{0-p} \leq a_{max}$), respectively. As can be observed in Fig. 12, chatter occurs regardless of the spindle speeds when the cutting width is 1.4 mm, and the experimental results represent higher stability than the predicted stability limit especially in the high-speed region (2500 min^{-1} and 3000 min^{-1}). This may come from the change of the specific cutting force in the wide cutting speed range, i.e., the specific cutting force generally decreases with the increase of the cutting speed. Meanwhile, it can be confirmed that the predicted stability limits with measured and fitted compliances are almost equal, and the predicted and measured chatter frequencies are all in good agreement; hence, the modal parameters can be used in the time-domain simulation with SSV.

Table 5. Experimental conditions for cutting with CSS.

Workpiece properties

Material		Brass CuZn35
Diameter D	[mm]	70
Specific cutting force in principal direction K_y	[MPa]	1284
Specific cutting force in thrust direction K_z	[MPa]	711
Tool properties		
Width (feed dir.) × Height (cutting dir.)	[mm]	25×15
Projection length	[mm]	80
Cutting condition		
Feed rate (static depth of cut) h_0	[mm/rev]	0.05
Cutting width a	[mm]	0.8, 1.0, 1.2, 1.4
Spindle speed n	[min^{-1}]	1000 - 3000

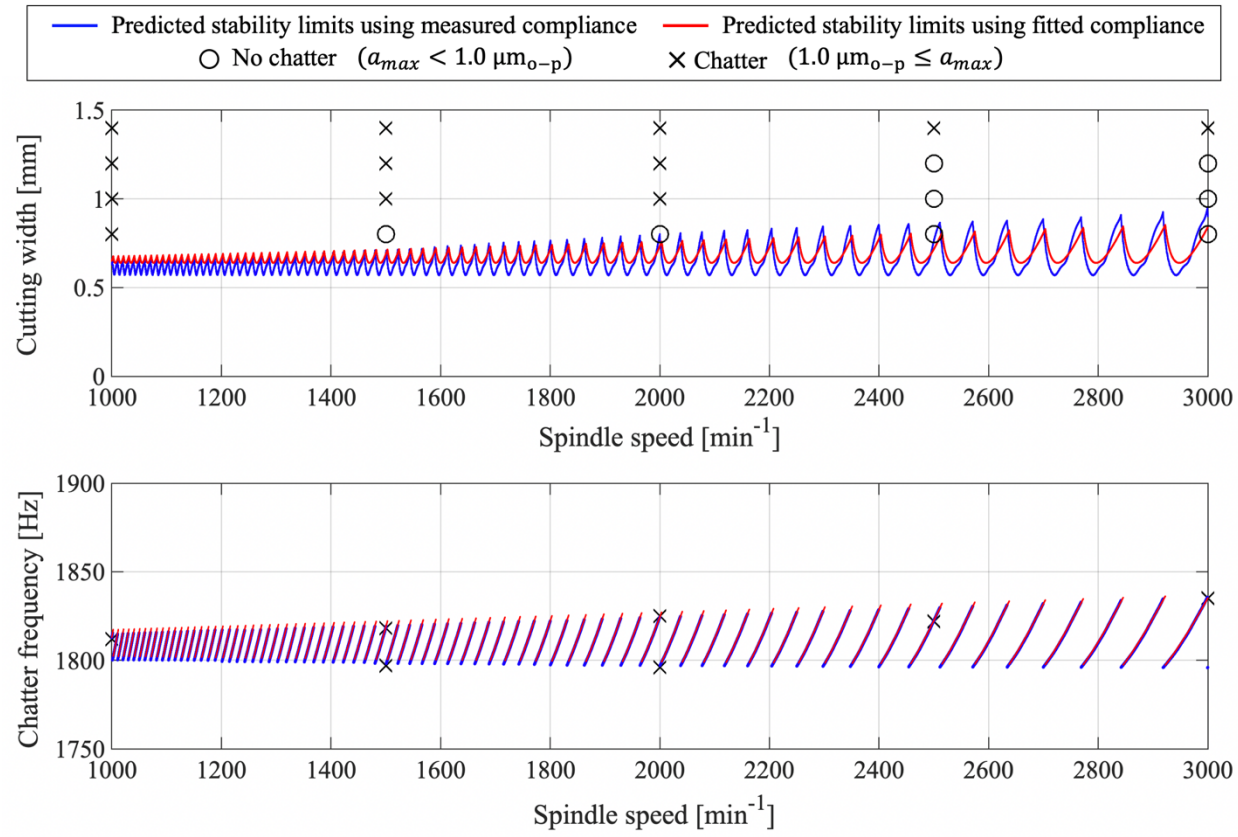

Fig. 12. Predicted stability limits and experimental results of CSS.

4.4 Method for generating CAR-SSV profile and experimental conditions

Cutting experiments with CAR-SSV and TSSV are carried out to verify the effectiveness of CAR-SSV as well as to confirm the relations between the parameters of CAR-SSV and the stability. The experimental conditions are shown in Table 6. Experiments with TSSV are carried out by utilizing a commercially available function (Okuma Corp., Machining Navi L-*g*). Note that the variation amplitude ratio RVA, which is defined as the ratio of the speed variation amplitude to the average spindle speed $n_{A,T}/n_{ave}$, is limited to 0.5 or lower. The values of the parameters of CAR-SSV and TSSV specified in

Table 6 represent the set values, and the actual values are directly measured from the obtained spindle speed signals.

Table 6. Experimental conditions for cutting with CAR-SSV and TSSV.

Parameters of CAR-SSV		
Reference spindle speed $n_{0,C}$	[min^{-1}]	1000, 1500, 2000
Variation period T	[s]	0.5, 1.0, 2,0, 4.0
Set acceleration rate r_s	[%]	1.0 – 6.0
Parameters of TSSV		
Nominal spindle speed $n_{0,T}$	[min^{-1}]	1000, 2000
Variation period T	[s]	1.0, 2.0, 4.0
Variation amplitude ratio RVA		0.1 - 0.5
Cutting conditions		
Feed rate (static depth of cut) h_0	[mm/rev]	0.05
Cutting width a	[mm]	1.0 - 5.0

Since CAR-SSV, which maintains a constant absolute acceleration rate, cannot be realized by existing NC commands, specially designed cutting experiments are conducted. The dummy turret of the CNC lathe shown in Fig. 9 is utilized to control the spindle speed. The spindle speed is controlled by the constant peripheral speed control function in which the spindle speed changes according to the x-axis position of the dummy turret. Here, the dummy turret is moved in accordance with previously prepared commands so that $\overline{|r_a|}$ is kept constant in the acceleration/deceleration section. For example, the spindle speed at the k-th revolution at a certain spindle rotational angle n_k [min^{-1}] can be expressed by Eq. (31) using the set constant peripheral speed V [m/min] and the distance from the center of the workpiece to the dummy turret at the k-th revolution R_k [mm] for the acceleration/deceleration section. In order to maintain $\overline{|r_a|}$ as r_s, the spindle speeds in two successive revolutions, i.e., n_k and n_{k-1}, should satisfy Eq. (5). From Eqs. (31) and (32), R_k can be calculated by Eq. (33).

$$n_k = \frac{1000V}{2\pi R_k} \tag{31}$$

$$n_k = \left(1 + \frac{r_s}{100}\right) n_{k-1} \tag{32}$$

$$R_k = \frac{R_{k-1}}{\left(1 + \frac{r_s}{100}\right)} \tag{33}$$

The dummy turret position in each revolution are calculated by utilizing Eq. (33), and they are interpolated with constant time steps.

An example of the experimental signals of the spindle speed, the acceleration rate, the spindle acceleration, the dummy turret position (x axis), the tool position (z axis), and the feed rate of the tool (z axis) at $n_{0,C} = 1000$ min^{-1}, $T = 4.0$ s, and $r_s = 2.0$ % are shown in Fig. 13. In order to calculate r_a, the spindle rotational angle is memorized in every moment, and then the moment of one revolution before as well as the spindle speed at that moment are determined. From the r_a profile, $\overline{|r_a|}$ is stably maintained as r_s in almost all sections except for the small overshoots near the sections where the acceleration direction switches. In addition, the feed rate of the tool is kept almost constant, and this denotes a constant static depth of cut. Every profile under each experimental condition is confirmed beforehand, and the conditions in which r_s can be stably maintained constant are selected for the cutting experiments. Since the original thickness of the pipe, i.e., the maximum cutting width, is 5.0 mm, the cutting width is varied from 1.0 mm to 5.0 mm with increments of 0.5 mm.

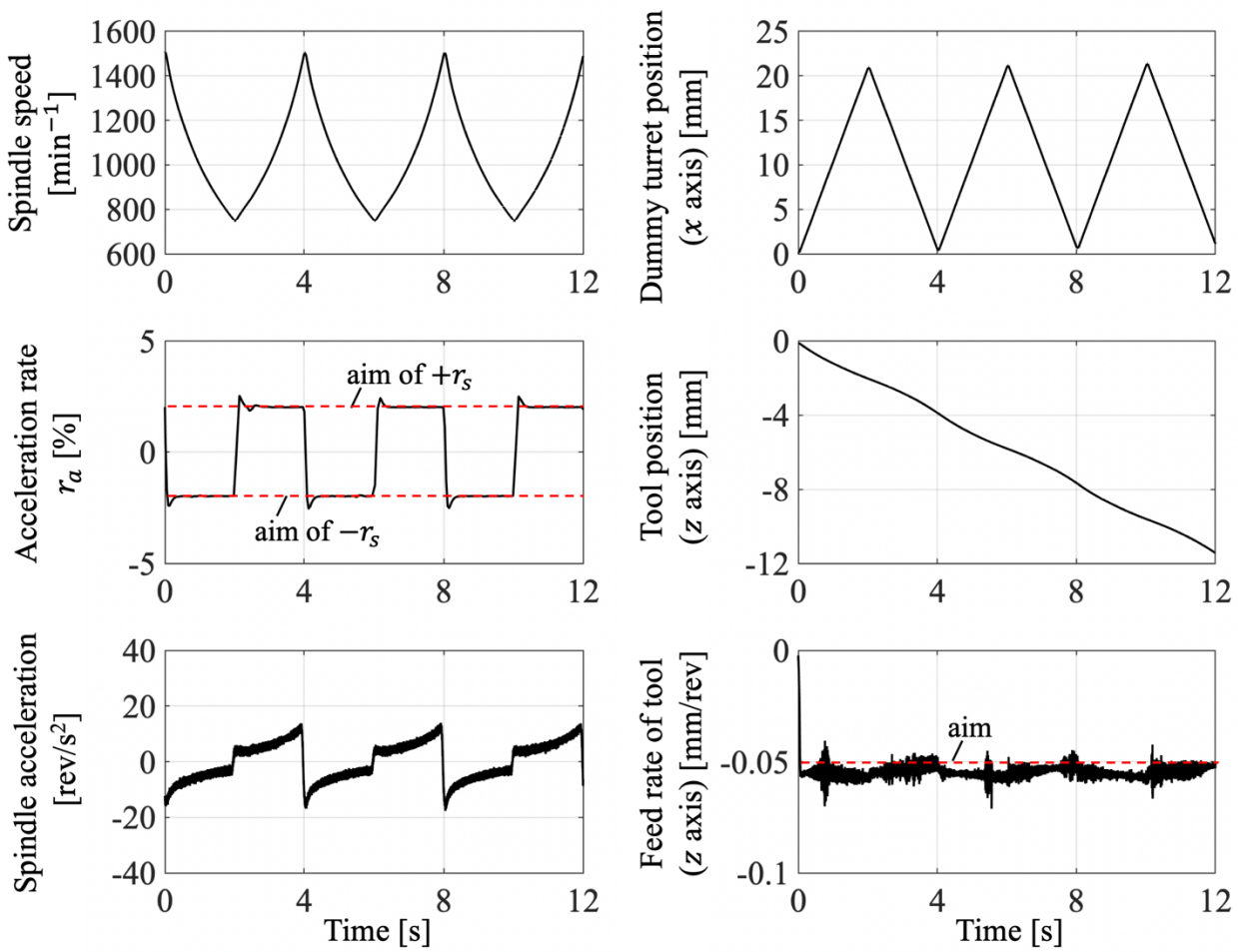

Fig. 13. Example of experimental signals of CAR-SSV at $n_{0,C} = 1000$ min^{-1}, $T = 4.0$ s, and $r_s = 2.0$ %.

4.5 Experimental results and discussions

Cutting experiments are carried out to confirm the validity of the analytical investigations with the time-domain simulation, and the experimental results are described with the same order in Chapter 3. Firstly, the stability of CAR-SSV is evaluated based on the stability indices $\overline{|r_a|}$ and N, and the results are shown in Fig. 14 under varied cutting widths: (a) 2.0 mm, (b) 3.0 mm, (c) 4.0 mm, and (d) 5.0 mm. The blue circles represent the cutting results without chatter ($a_{max} < 1.0$ μm$_{0-\mathrm{p}}$), and the red crosses represents the cutting results with chatter (1.0 μm$_{0-\mathrm{p}} \leq a_{max}$). Since the maximum cutting width is 5 mm because of the original thickness of the pipe, the stable experimental results at 5 mm mean that the actual stability limit is over 5 mm. $\overline{|r_a|}$ and N are directly calculated from the measured spindle speed signals. From Fig. 14, the following remarks which have been found from the simulation are confirmed as follows:

1) When N is almost the same, the stability increases with an increase of $\overline{|r_a|}$. Especially, when $\overline{|r_a|}$ is near 4 %, chatter is stably suppressed under all N even if the cutting width is set to 5.0 mm, which is 4 times the asymptotic stability limit of CSS. Therefore, it can be said that $\overline{|r_a|}$ is an effective stability index in CAR-SSV.
2) When $\overline{|r_a|}$ is almost the same, the stability increases with an increase of N. For example, when $\overline{|r_a|}$ is almost equal to or higher than 2 % and N is higher than 10, chatter is stably suppressed even if the cutting width is set to 5.0 mm. Hence, it can be said that N is also an effective stability index in

CAR-SSV.
Consequently, it is desirable to set higher $\overline{|r_a|}$ and N to achieve higher stability.

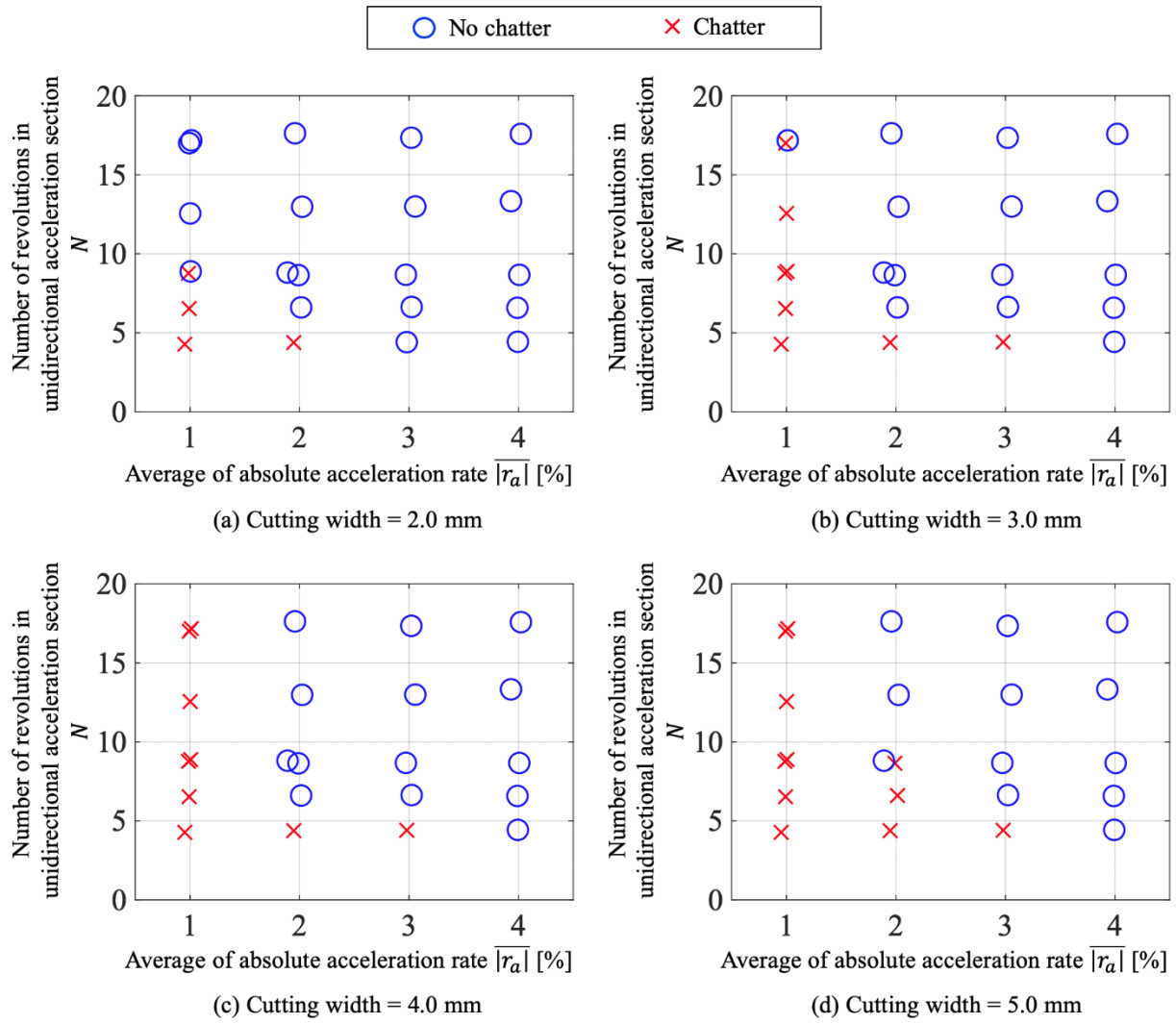

Fig. 14. Results of cutting experiments in CAR-SSV against stability indices $\overline{|r_a|}$ and N under varied cutting width.

Secondly, the relations between the parameters of CAR-SSV and the stability are investigated. The results of the cutting experiments and the time-domain simulations are shown in Fig. 15. Figs. 15(a)-15(f) show the results under varied conditions of $n_{0,C}$ and T: (a) $n_{0,C} = 1000$ min^{-1}, $T = 0.5$ s, (b) $n_{0,C} = 1000$ min^{-1}, $T = 1.0$ s, (c) $n_{0,C} = 1000$ min^{-1}, $T = 2.0$ s, (d) $n_{0,C} = 1500$ min^{-1}, $T = 0.5$ s, (e) $n_{0,C} = 1500$ min^{-1}, $T = 1.0$ s, and (f) $n_{0,C} = 1500$ min^{-1}, $T = 2.0$ s. Note that the measured spindle speed signals and the identified modal parameters shown in Table 4 are utilized in the time-domain simulations. The horizontal and vertical axes represent the set acceleration rate r_s and the cutting width, respectively. The blue dotted line with squares represents the predicted stability limit. Since the acceleration rate cannot be maintained nearly constant at $n_{0,C} = 1500$ min^{-1}, $T = 2.0$ s, and $r_s = 4$ %, this condition is excluded. As shown in Fig. 15, it can be confirmed that the experimental results show higher stability than the predicted ones. This is consistent with the results of CSS shown in Fig. 12. In addition, the tendency of the stability within the experiments and within the simulations are consistent. The following remarks which have been found from the simulation are confirmed as follows:

1) The higher r_s, the higher the stability under the conditions with the same $n_{0,C}$ and T. Especially, when r_s is 4.0 %, the whole thickness of the pipe, i.e., 5 mm, which is about 3.5 times the maximum stability limit in CSS, is cut without chatter regardless of $n_{0,C}$ and T. Hence, it is desirable to set a larger r_s, without exceeding the limit of the spindle motor load, to obtain higher stability.
2) When r_s and $n_{0,C}$ are the same, the higher T, the higher the stability (see Figs. 15(a)-15(c) and 14(d)-14(f)). In the same manner, when r_s and T are the same, the higher $n_{0,C}$, the higher the stability (see Figs. 15(a) and 15(d), 15(b) and 15(e), and 15(c) and 15(f)). As described in the analytical investigations, the reasons for these tendencies can be explained as follows. The larger T and $n_{0,C}$ under the same r_s, the larger $\overline{|r_a|}$ and N, and hence the stability becomes higher. It is experimentally verified that CAR-SSV is an effective solution to overcome the limitation of conventional SSV.
3) The increase of the stability against the increase of T becomes small at $n_{0,C} = 1500$ min^{-1} (see Figs. 15(e) and 15(f)). The reduction effect of the dynamic compliance reaches a certain asymptotic value since the compliance is nearly constant far away from the resonance. Therefore, there is a limitation in the stabilizing effect from the increase of T.

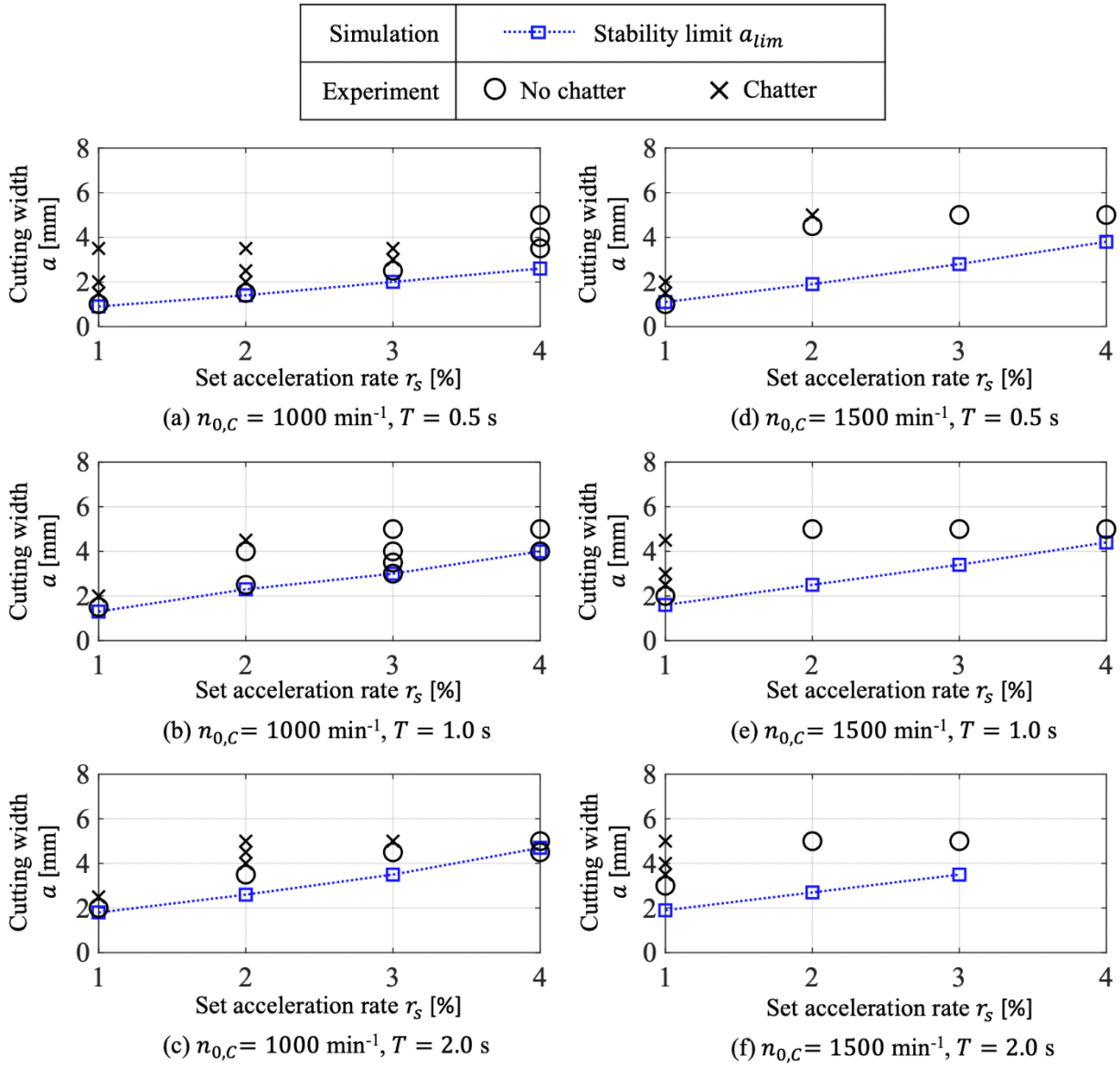

Fig. 15. Results of cutting experiments and time-domain simulation in CAR-SSV against set acceleration rate r_s under varied $n_{0,C}$ and T.

Finally, in order to verify the effectiveness of CAR-SSV focusing on its applicability to the actual industry, a comparison between CAR-SSV and TSSV is conducted considering the thermal load of the spindle. As shown in Section 3.2, the machining efficiency against the thermal load of the spindle motor is compared between the two profiles. The average of the square of the spindle acceleration $\bar{H}$ [rev^2/s^4] is utilized as a proportional value to the average thermal load of the spindle motor. $\bar{H}$ is calculated from the measured spindle speed signal. The average spindle speed of CAR-SSV $n_{ave,C}$ and TSSV $n_{ave,T}$ are also calculated from the measured spindle speed signal, and they are utilized for the calculation of the machining efficiency, i.e., material removal rate (MRR), P [mm^3/min] expressed in Eq. (29). Fig. 16 shows the results of P against $\bar{H}$ under varied T's: (a) T = 1.0 s, (b) T = 2.0 s, and (c) T = 4.0 s. The red circles and blue triangles represent the results of CAR-SSV and TSSV, respectively. The stability limit is determined from the results shown in Fig. 15, and it is utilized for the calculation of P. As in the other experiment, the condition where the maximum thickness of the pipe (5.0 mm) is stably cut is excluded. In addition, the conditions where the profile of TSSV cannot be generated due to the limitation of RVA are excluded. In

Fig. 16, an increase of $\overline{H}$ means an increase of the acceleration, and hence RVA of TSSV and r_s of CAR-SSV take higher values with higher $\overline{H}$. Fig. 17 shows examples of the experimental signals of the spindle speed, the acceleration rate, the vibration acceleration obtained from accelerometer, and the short-time Fourier transform results of the vibration acceleration for the profiles marked as A and B on Fig. 16: (a) CAR-SSV ($a = 3.5$ mm, $\overline{H} = 39.51$ rev^2/s^4, $n_{ave,C} = 1014$ min^{-1}, $T = 2.0$ s, and $r_s = 2.0$ %) and (b) TSSV ($a = 2.5$ mm, $\overline{H} = 38.70$ rev^2/s^4, $n_{ave,T} = 1002$ min^{-1}, $T = 2.0$ s, and $RVA = 0.2$). From Figs. 16 and 17, the following remarks which have been found in the simulation are confirmed as follows.

1) When $\overline{H}$ is almost the same, the machining efficiency is increased by utilizing CAR-SSV under all conditions. Therefore, it is experimentally verified that the effectiveness of CAR-SSV is superior to that of TSSV considering the motor load.
2) As shown in Fig. 17, although the cutting width of CAR-SSV (A of Fig. 16) is 40% larger than that of TSSV (B of Fig. 16), the vibration amplitude in CAR-SSV is extremely small except for the vibration at the beginning of the cutting caused by the initial cutting force input. On the other hand, in the case of TSSV, the growth of the vibration with a decrease of $|r_a|$ can be observed where the acceleration direction switches. From these results, it can be concluded that the superior chatter suppression effect of CAR-SSV is verified experimentally.

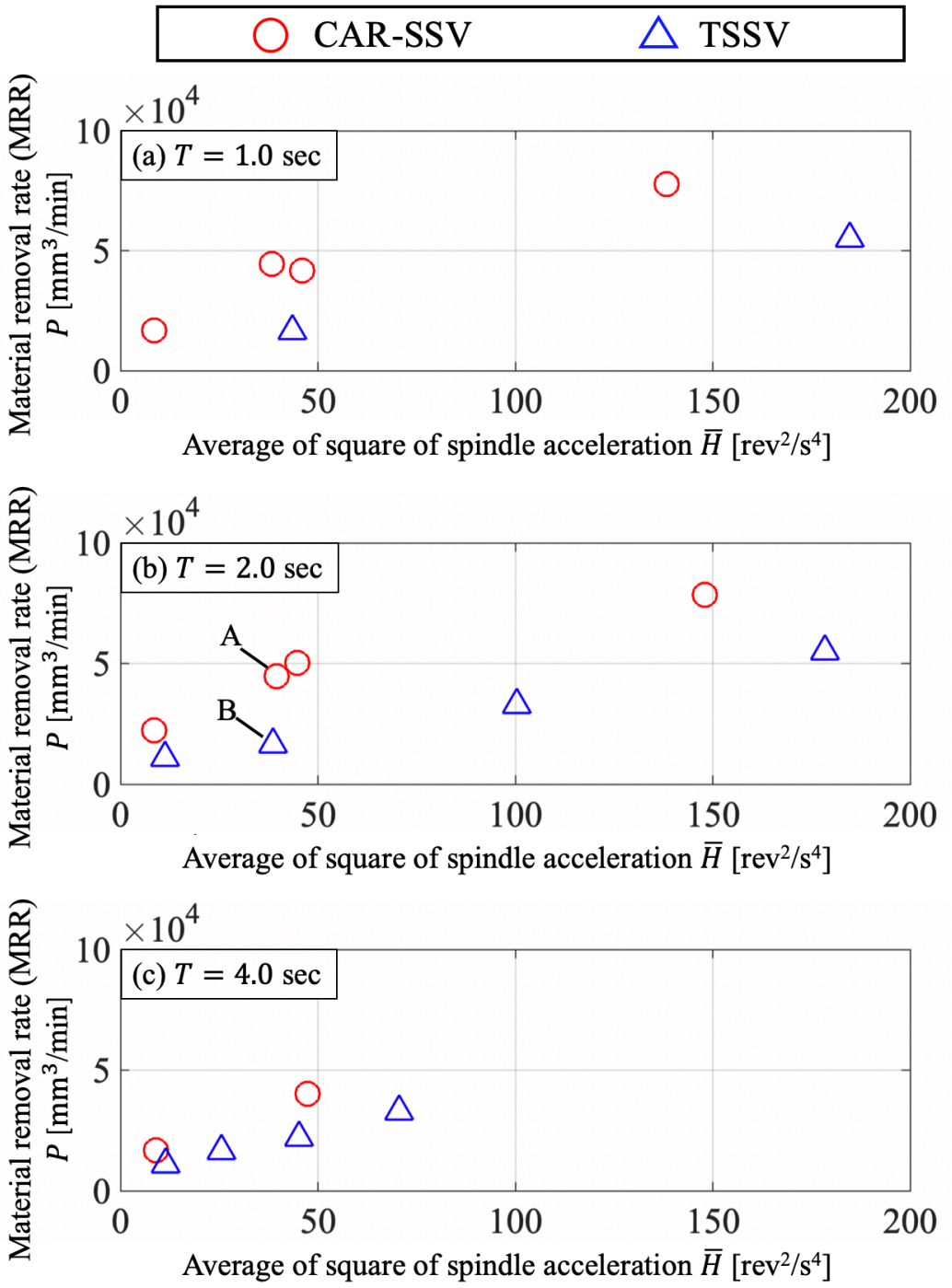

Fig. 16. Experimental results of material removal rate (MRR) P [mm^3/min] against average of square of spindle acceleration $\bar{H}$ [rev^2/s^4] under varied T: (a) T = 1.0 s, (b) T = 2.0 s, and (c) T = 4.0 s.

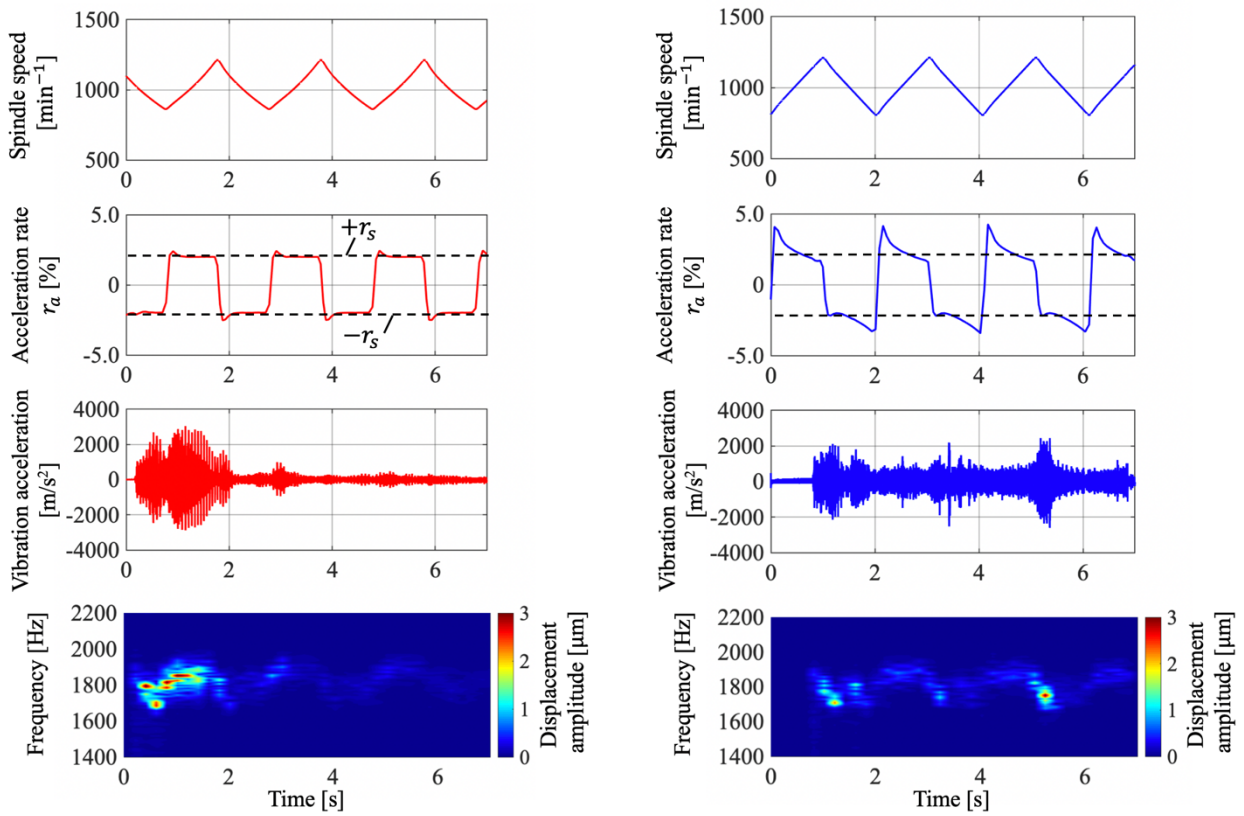

(a) CAR-SSV (A of Fig. 15) (b) TSSV (B of Fig. 15)

Fig. 17. Example of experimental signals of spindle speed and acceleration rate, corresponding vibration acceleration obtained from accelerometer, and short-time Fourier transform result of vibration acceleration under cutting conditions marked as A and B on Fig. 16: (a) CAR-SSV ($a = 3.5$ mm, $\bar{H} = 39.51$ rev^2/s^4, $n_{ave,C} = 1014$ min^{-1}, $T = 2.0$ s, and $r_s = 2.0\%$) and (b) TSSV ($a = 2.5$ mm, $\bar{H} = 38.70$ rev^2/s^4, $n_{ave,T} = 1002$ min^{-1}, $T = 2.0$ s, and $RVA = 0.2$).

5 Conclusion

A new SSV profile, which was named CAR-SSV (SSV with constant acceleration rate), is proposed to overcome the limitation of the chatter stability improvement in conventional SSV. Since the absolute acceleration rate is maintained a constant, chatter suppression throughout the cutting can be achieved.

Analytical investigation was conducted to reveal the potential of the proposed profile. Firstly, the relations between the stability limit and the proposed stability indices in SSSV, TSSV, and CAR-SSV were investigated, and the results of CAR-SSV were compared with those of SSSV and TSSV. From the investigation, the following remarks were found.

1) When $\overline{|r_a|}$ and N are the same, the stability limit of CAR-SSV is always equal to or higher than those of SSSV and TSSV. The larger the $\overline{|r_a|}$ and N, the larger the increase of the stability limit.
2) When N is the same, the stability limit increases with an increase of $\overline{|r_a|}$.
3) When $\overline{|r_a|}$ is the same, the stability limit of CAR-SSV increases with an increase of N under all $\overline{|r_a|}$.

Secondly, the following relations between the parameters of CAR-SSV and the chatter stability were revealed:

1) The stability increases with a higher r_s, and hence it is desirable to set a larger r_s under the imposed limitation of the spindle motor load.
2) When r_s is the same, the stability limit increases with larger $n_{0,C}$ and T in most cases. This is because the larger T and $n_{0,C}$, the larger $\overline{|r_a|}$ and N. This denotes that CAR-SSV can be an effective solution since the machining efficiency increases with higher T and $n_{0,C}$, i.e., higher stability limit (cutting width).
3) The increase of the stability with higher $n_{0,C}$ is small under a long T. Because the reduction effect of the dynamic compliance reaches a certain asymptotic value since the compliance is nearly constant far away from the resonance. Consequently, there is a limitation for the improvement of the stability with an increase of $n_{0,C}$ and T.

Thirdly, to verify the effectiveness of CAR-SSV considering its applicability to the actual industry, the machining efficiency P, i.e., material removal rate (MRR), against the thermal load of the spindle motor $\overline{H}$ was compared with the conventional SSV profiles. The results were summarized as follows:

1) When $\overline{H}$ is the same, P of CAR-SSV is equal to or higher than that of conventional SSV in most conditions.
2) The increase of P by utilizing CAR-SSV becomes larger with larger $\overline{H}$ and T. The larger the $\overline{H}$ and T, the larger the fluctuation amplitude of r_a in TSSV and SSSV, and the sections become longer where $|r_a|$ in TSSV and SSSV is smaller than $|r_a|$ in CAR-SSV. Hence, the stabilization effect decreases in TSSV and SSSV since a sufficient compliance reduction cannot be obtained.

A series of experiments were carried out to confirm the relations between the parameters of CAR-SSV and the stability as well as to verify the effectiveness of CAR-SSV. Since CAR-SSV cannot be realized by existing NC commands, specially designed cutting experiments were conducted.

The stability of CAR-SSV was evaluated based on the stability indices $\overline{|r_a|}$ and N. When N is almost the same, the stability increases with an increase of $\overline{|r_a|}$. Next, when $\overline{|r_a|}$ is almost the same, the stability increases with an increase of N. Hence, it can be said that $\overline{|r_a|}$ and N are effective stability index.

The experimental results showed that a higher stability can be obtained by setting a higher r_s, and this is consistent with the results of the simulation. Especially, when r_s is 4.0 %, the whole thickness of the pipe, which is 3.5 times larger than the maximum stability limit in CSS, was stably cut. Next, when r_s and $n_{0,C}$ are the same, a higher stability was obtained with a higher T. In addition, when r_s and T are the same, a higher stability was obtained with a higher $n_{0,C}$. These results were exactly the same with the analytical results. From these results, it was verified that a remarkable improvement of the machining efficiency can be realized by utilizing CAR-SSV, and CAR-SSV is an effective solution to overcome the limitation of conventional SSV.

From the comparison between CAR-SSV and TSSV focusing on their practicality, higher machining efficiency was obtained by utilizing CAR-SSV under all conditions. These results indicate that the superior effectiveness of CAR-SSV when considering the motor thermal load was experimentally verified. Furthermore, although the cutting width in CAR-SSV was set 40 % larger than TSSV, the vibration amplitude diminished when utilizing CAR-SSV, and the amplitude near the end of cutting was extremely smaller than that in TSSV. On the other hand, in the case of TSSV, the growth of the vibration with a decrease of $|r_a|$ was observed at the transitions from acceleration to deceleration. Therefore, it was verified that CAR-SSV can effectively suppress chatter throughout the cutting when r_s is set larger than the critical value. From these results, it can be concluded that CAR-SSV is a valid solution to overcome the limitation of conventional SSV.

References

[1] Tobias S. A., Fishwick W. Theory of regenerative machine tool chatter. The engineer 1958; 205.7: 199-203.

[2] Quintana G., Ciurana J. Chatter in machining processes: A review. International Journal of Machine Tools and Manufacutre, 2011; 51(5), 363-376.

[3] Zhu L., Liu C. Recent progress of chatter prediction, detection and suppression in milling. Mechanical Systems and Signal Processing 2020; 143, 106840.

[4] Marui E., Ema S., Hashimoto M., and Wakasawa Y. Plate insertion as a means to improve the damping capacity of a cutting tool system. International Journal of Machine Tools and Manufacture, 1998; 38(10-11):1209-1220.

[5] Shamoto E., Kageyama K., Moriwaki T. Suppression of regenerative chatter vibration with irregular pitch end mill- construction of analytical model and optimization of pitch angle. Proceedings of JSME Kansai Branch Annual Meeting 2002; 024(1).

[6] Hayasaka T., Ito A., Shamoto E. Generalized design method of highly-varied-helix end mills for suppression of regenerative chatter in peripheral milling. Precision Engineering 2016; 48:45-59.

[7] LIN S. C., HU M. R., Low vibration control system in turning. International Journal of Machine Tools and Manufacture 1992; 32.5: 629-640.

[8] MEI Z., Yang S., Shi H., Chang S., Ehmann K.F. Active chatter suppression by on-line variation of the rake and clearance angles in turning-principles and experimental investigations. International Journal of Machine Tools and Manufacture 1994; 34.7: 981-990.

[9] Wan S., Li X., Su W., Yuan J., and Hong J. Active chatter suppression for milling process with sliding mode control and electromagnetic actuator. Mecahnical Systems and Signal Processing 2020; 136:106528.

[10] Dohner Jeffrey L., et al. Mitigation of chatter instabilities in milling by active structural control. Journal of sound and vibration 2004; 269.1-2: 197-211.

[11] Tsao TC., McCarthy MW., Kapor SG. A new approach to stability analysis of variable speed machining systems. International Jounal of Machine Tools and Manufacture 1993; 33(6): 791-808.

[12] Al-Regib E., Ni J., Lee S. H. Programming spindle speed variation for machine tool cahtter suppression. International Journal of Machine Tools and Manufacture 2003; 43(12): 1229-1240.

[13] Otto A., Radons G. Application of spindle speed variation for chatter suppression in turning. CIRP Journal of Manufacturing Science and Technology 2013; 6(2): 102-109.

[14] Hayasaka T., Nam S., Jung H., Shamoto E., Saito K. Proposal of ‘accelerative cutting‘ for suppression of regenerative chatter. CIRP Annals 2018; 67(1): 401-404.

[15] Nam S., Hayasaka T., Jung H., Shamoto E. Proposal of novel chatter stability indicies of spindle speed variation based on ist chatter growth characteristics. Precision Engineering 2020; 62: 121-133.

[16] Kondo Y., Kawano O., and Sato H., Behavior of self-excited chatter due to multiple regenerative effect. Journal of Engineering for Industry 1981; 324-329.

[17] Suzuki N, Nishimura K, Shamoto E, Yoshino K. Effect of cross transfer function on chatter stability in plunge cutting. Journal of Advanced Mechanical Design Systems and Manufacturing 2010; 4(5):883-891.